

# THERMAL CONDUCTIVITY IN MAGNETIC SUPERCONDUCTORS

B. I. Belevtsev<sup>\*1</sup>, B. D. Hennings<sup>†</sup>, K. D. D. Rathnayaka<sup>†</sup>, and D. G. Naugle<sup>†2</sup>

<sup>\*</sup>B. Verkin Institute for Low Temperature Physics and Engineering, National Academy of Sciences, Kharkov 61103, Ukraine

<sup>†</sup>Physics Department, Texas A&M University, College Station, TX 77843-4242, USA

## I. INTRODUCTION

The thermal conductivity is a property that can provide significant information about the nature of superconductors. Even in the early studies of high- $T_C$  superconductors before good single crystal samples were available, thermal conductivity results indicated the anomalous behavior of the normal state transport properties of these oxides and many properties of their superconducting state. (See Uher [1] for a review of early thermal conductivity studies in the high- $T_C$  superconductors.) Recent low temperature thermal conductivity measurements in the normal state of an overdoped cuprate superconductor  $Tl_2Ba_2CuO_{6+\delta}$  [2] have demonstrated that the fermions which carry heat also carry charge

---

<sup>1</sup> E-mail: belevtsev@ilt.kharkov.ua

<sup>2</sup> E-mail: naugle@physics.tamu.edu

(i.e. the Wiedemann-Franz law is fully obeyed, thus providing no evidence for spin-charge separation in overdoped high- $T_C$  compounds). In contrast, this same group has observed a breakdown of the Wiedemann-Franz law at low temperatures (below  $T_0 \approx 0.15$  K) in a different high- $T_C$  cuprate ( $\text{Pr}_{2-x}\text{Ce}_x\text{CuO}_{4-\delta}$ ) near the optimal doping [3] which suggests that superconductivity in the underdoped region of the phase diagram may indeed be the result of charged bosons rather than the Cooper pairing most likely responsible for superconductivity in the overdoped regime. It was pointed out in Ref. [4], however, that the experiments of Hill *et al.* [3] leave room for possibility that charge-carrying excitations are fermionic, but that a subtle transition occurs at  $T_0$ . In any case, such experiments help to indicate the value of thermal conductivity measurements to probe the fundamental properties of new materials.

The focus of this work is thermal conductivity measurements in systems that appear to exhibit microscopic coexistence of magnetic and superconducting order, two types of ordering that are generally antagonistic. Although the traditional transport coefficients, Hall effect, thermopower and resistivity, provide little or no information in the superconducting phase below  $T_C$ , thermal conductivity measurements can still probe both the phonons and, at least for a reasonable range of temperature below  $T_C$ , the electron quasi-particles which are the two primary heat carriers in a superconductor. This may be particularly useful for magnetic superconductors in the situation where the magnetic ordering temperature  $T_M$  is less than the superconducting temperature  $T_C$  since the electron contribution and, perhaps to a lesser extent, the phonon contribution, may both be influenced by the magnetic ordering. At high temperature the thermal conductivity also provides information regarding the scattering processes for these carriers and, as will be illustrated, can provide indications of subtle high temperature phase transitions. Thus, thermal conductivity can be an important tool for study of new materials over the entire temperature range.

In the 1980's, discovery of the microscopic coexistence of both ferromagnetic and antiferromagnetic order in the presence of superconducting order in various Chevrel phase and rare earth rhodium boride compounds led to a new view of these two antagonistic phases. The experiments generated great excitement, and a large number of theoretical predictions of new types of order involving spatial modulation of the two very different, mutually exclusive order parameters appeared. Difficulty in synthesis of high quality samples of these magnetic superconductors coupled with the excitement of the discovery of superconductivity above the boiling point of liquid nitrogen in high- $T_C$  oxide superconductors led to greatly reduced activity in this field. (See Maple [5], Bulaevskii *et al.* [6] and Fischer [7] for excellent reviews of the state of experiment and theory in

that era.) The discovery [8–11] of the family of rare earth nickel borocarbide ( $\text{RNi}_2\text{B}_2\text{C}$ ) superconductors, which exhibit such a wide variety of interesting phenomena, and the widespread availability of good single crystal samples [12] has led to renewed interest in questions regarding the coexistence of superconductivity and magnetic order. This family exhibits superconducting order only ( $\text{R} = \text{Y}, \text{Lu}$ ), heavy fermion behavior ( $\text{R} = \text{Yb}$ ), coexistence of superconductivity and magnetic order ( $\text{R} = \text{Tm}, \text{Er}, \text{Ho}, \text{Dy}$ ) and magnetic order only ( $\text{R} = \text{Tb}, \text{Gd}$ ) within the same crystal structure. Although we have not found any thermal conductivity measurements in the literature for the Chevrel and rare earth rhodium boride magnetic superconductors, perhaps due to the difficulty of sample preparation, rather complete data now exists for single crystals of the rare earth nickel borocarbides. There are indications of coexistence of magnetic order and superconductivity in a new system, the 2122 phase of rare earth rutheno-cuprates, also. So far there appears to be only one report [13] of thermal conductivity, in an oxygen rich  $\text{Eu}_{1.5}\text{Ce}_{0.5}\text{RuSr}_2\text{Cu}_2\text{O}_{10-\delta}$  compound, but the results of this study suggest strongly coupled weak ferromagnet-antiferromagnet/superconductor-normal metal transitions at a remarkably high temperature ( $\approx 45 \text{ K}$ ).

A brief discussion of the experimental considerations is given in section II with a review of the theoretical aspects given in section III. Measurements of the thermal conductivity, together with some illustrative data from thermopower and resistivity measurements, for the borocarbides and the rutheno-cuprate are discussed in section IV. Section V presents a short conclusion. The reader reasonably familiar with thermal conductivity and interested primarily in the results for magnetic superconductors may go directly to section IV.

## II. EXPERIMENTAL TECHNIQUES

We will consider in the following, mainly, the thermal conductivity measurements made in the Low Temperature Laboratory at Texas A&M University. For this reason, we will describe below in sufficient detail the technique employed in this lab. This technique is, however, essentially the same as that used in many other labs for low temperature measurements of the thermal conductivity. A more general and thorough account of available methods of thermal conductivity measurements can be found in Refs. [14, 15]

The thermal conductivity of samples was measured by the steady state linear heat flow method. One end of the sample was thermally isolated (a known, constant heat input via a resistive heater was applied to that end), and the resultant steady state temperature gradient was measured. The temperature difference,  $\Delta T$ , between the two ends of the sample (which was typically less than 5% of the absolute temperature) was measured with

a Au-0.007 at. %Fe – Chromel thermocouple. Verification of the temperature difference was provided by a Chromel-Constantan thermocouple for most of the temperature range. The temperature differences for each sample and the calibration samples (silver foils) were chosen to be approximately the same in the different temperature ranges. The sample was completely surrounded by a thermal shield held at the temperature of the cold end. Even though heat leaks were minimized by design, the actual heat leaks were measured and accounted for in the thermal conductivity data. All this suggests an absolute accuracy for the thermal conductivity of  $\pm 3$  % with the relative precision of  $\pm 3$  % on a specific measurement run. The value of the thermal conductivity  $\kappa(T)$  is calculated using the relation

$$\kappa(T) = \frac{L}{A} \frac{\dot{Q}}{\Delta T}, \quad (1)$$

where  $L$  and  $A$  are length and cross-sectional area of the sample,  $\dot{Q}$  is the power input. A detailed discussion of the thermal-conductivity measurement technique employed can be found in [16].

The above-indicated instrumental error in the thermal conductivity measurements should be considered as the optimum or, better to say, minimum one. Some reservations, therefore, should be added to this. First, it is usually more difficult to make a good thermal contact to an oxide sample than to a metallic one. A somewhat greater inaccuracy can be expected in the former case. Second, all the thermal conductance measurements were made in a vacuum of  $1 \times 10^{-6}$  Torr or better, so the convective heat losses are negligibly small. The radiative heat losses, due to the small temperature difference between the base  $T$ -end and the  $\Delta T$ -end of the sample mentioned above, should be small except perhaps at higher temperatures. As was pointed out in Refs. [1, 14], this radiation loss can lead to an overestimate of the measured thermal conductivity above  $T \approx 150$  K, and the error grows with increasing temperature. Measurement of the actual heat leaks without sample, as in the present case, provides partial correction for this error. Lastly, it is seen from Eq. (1) that an appreciable error in the absolute determination of the thermal conductivity (as well as in supporting measurements of electrical resistivity) is due to inaccuracies in the sample dimension measurements. Taking all this into account, it can be said that the absolute accuracy for borocarbide and rutheno-cuprate samples can be worse than  $\pm 3$  %, primarily due to inaccuracies in determination of the geometric factors of the somewhat irregular single crystal samples and contact resistance for the pressed powder rutheno-cuprate samples.

The electrical resistivity,  $\rho(T)$ , was measured for all of the samples studied (except the rutheno-cuprate) using the standard four-terminal method. These measurements are

helpful and even imperative in many respects. First of all, it gives an indication of the quality of the sample. Second,  $\rho(T)$  curves have in general some peculiarities at magnetic transitions and show the resistive transition at the superconducting transition temperature,  $T_C$ . Last but not least,  $\rho(T)$  data allow use of the Wiedemann-Franz law to estimate the fraction of the total thermal conductivity, that is due to the charge-carrier contribution, and, hence, the remainder can be thought to be due to phonons and magnetic effects, if any. In the case of rare-earth nickel borocarbides, both the resistivity and thermal conductivity were measured in the  $ab$ -plane.

### III. THEORETICAL CONCEPTS

For consideration and discussion of available thermal conductivity data for the magnetic superconductors, we will refer to the well established physical mechanisms for heat transfer in normal metals and superconductors, outlined in well known books or papers [1, 14, 17–27]. With this we will try to understand and explain what is observed in magnetic superconductors and make some conclusions about the properties of heat carriers in them. Since the main heat carriers in conducting solids are charge carriers (electrons or holes) and lattice thermal excitations (phonons), the thermal conductivity behavior reflects properties of these quasiparticles and an interaction between them. In magnetic states the magnetic excitations (i.e. magnons) can also participate in the heat transport. Hence the thermal conductivity measurements can provide an insight into the nature of the superconducting and magnetic states of magnetic superconductors.

The main (and sometimes rather difficult) task in an analysis of the thermal conductivity data for some particular material is to separate the contributions from the two main type of the heat carriers – electrons and phonons. This requires, primarily, a knowledge about an expected temperature behavior of these contributions (which are quite different for electron and phonon heat carriers). Crystal-lattice disorder can strongly effect both the electron and phonon parts of thermal conductivity and, therefore, must generally be considered. Generally speaking, it is important to find out what scattering mechanism limits the heat transport for given channel (electrons/phonons) at given conditions, which are determined by the phase or state of a sample, its temperature, the magnitude of applied magnetic field and other circumstances.

In the simplest way the thermal conductivity of any type of heat carriers can be presented by the equation [14, 17, 19, 20]

$$\kappa(T) = \frac{1}{3}C_v\bar{v}l = \frac{1}{3}C_v\bar{v}^2\tau, \quad (2)$$

where  $C_v$  is the heat capacity per unit volume at constant volume,  $\bar{v}$  is the average velocity of the heat carriers,  $l$  is the mean free path of the heat carriers (that is the average distance they travel between the collisions with any obstacles to heat transport), and  $\tau$  is the corresponding relaxation time. Since the quantity  $D = (1/3)\bar{v}l$  is just a diffusion coefficient of the heat carriers, it can be said that the thermal conductivity is determined by the heat capacity and diffusivity of the heat carriers. In line with this, its temperature dependence,  $\kappa(T)$ , is determined by those of the heat capacity and the mean free path of the heat carriers, since  $\bar{v}$  is essentially temperature independent (although it can undergo a change at some phase transitions).

Eq. (2) is applicable for both electron and phonon heat transport in solids. Generally, the heat transport via electrons and phonons occurs in parallel. It can be written then

$$\kappa = \kappa_p + \kappa_e, \quad (3)$$

where  $\kappa_p$  and  $\kappa_e$  present the contributions from the phonons and free charge carriers, respectively. Below we consider these contributions separately. The phonon heat transport takes place in any solid; whereas, the charge carrier contribution depends on the carrier density, and is, therefore, negligible in insulators. It should be noted as well that different types of relaxation processes, which act simultaneously, can limit the thermal and electrical conductivities. As a quite good approximation, Matthiessen's rule [17, 18], is applied in this case to describe the combined effect of these processes:

$$\frac{1}{\tau_{\text{eff}}} = \sum_i \frac{1}{\tau_s^i}, \quad (4)$$

where  $\tau_{\text{eff}}$  is the effective (or total) relaxation time, and the times  $\tau_s^i$  correspond to different relaxation processes. Since the mean free path is proportional to the relaxation time ( $l = \bar{v}\tau$ ), the same relation can be written for the effective mean free path,  $l_{\text{eff}}$ . According to the Matthiessen's rule, the electrical resistivity can be presented as a sum of the partial resistivities, corresponding to different processes of the electron scattering. By analogy, it is convenient in many cases to consider the thermal resistivity,  $W = 1/\kappa$ , [17, 20] as a sum of partial resistivities

$$1/\kappa_{\text{eff}} = W = \sum_i W_i \quad (5)$$

### A. Phonon thermal conductivity in non-metallic crystals

For phonon thermal conductivity, one can use in Eq. (2) the lattice specific heat  $C_p$ , and  $\bar{v}$  may be taken as an average velocity of sound,  $v_s$ . As a good approximation, the

Debye model for the lattice specific heat [17, 19] can be used. According to it,

$$C_p \propto T^3 \quad (T \ll \Theta_D), \quad (6a)$$

$$C_p = 3Nk_B \quad (T > \Theta_D), \quad (6b)$$

where  $N$  is the ion density. The main problem is to take into account the most important mechanisms of phonon relaxation in crystal solids. In doing so it is convenient to operate with the thermal resistivity, which can be presented in Matthiessen's approximation as

$$1/\kappa_p = W_p = W_{pp} + W_{pi} + W_{pe} = \frac{3}{C_p v_s^2} (\tau_{pp}^{-1} + \tau_{pi}^{-1} + \tau_{pe}^{-1}), \quad (7)$$

where subscripts **pp**, **pi** and **pe** indicate the phonon-phonon, phonon-imperfection and phonon-electron interactions, respectively.

The phonon-phonon and phonon-imperfection interactions, corresponding to the first two terms in Eq. (7), occur in any solid; whereas, the phonon-electron interaction can be important only in solids with fairly high charge-carrier density. Let us consider, at first, a rather perfect non-metallic crystal, where the main contribution to the thermal conductivity comes from the phonon-phonon interaction [14, 17, 19, 20]. These processes are those in which two phonons can combine to give a third, and vice versa (so called, three-phonon processes). They are restricted by the following selection rules:

$$\hbar\omega_1 + \hbar\omega_2 = \hbar\omega_3, \quad (8a)$$

$$\mathbf{q}_1 + \mathbf{q}_2 = \mathbf{q}_3 + \mathbf{g}, \quad (8b)$$

where the first condition is conservation of energy at the interaction. In the second condition for wave vectors of interacting phonons,  $\mathbf{g}$  is a reciprocal lattice vector. The case  $\mathbf{g} = 0$  corresponds to the conservation of momentum (or wave vector). These processes are called *Normal* processes or *N*-processes. The case  $\mathbf{g} \neq 0$  is determined by the interference condition for wave vectors (the lattice acts in that event as a diffraction grating). These processes are called *Umklapp* processes or *U*-processes.

Since *N*-processes are energy and momentum conserving they do not contribute to the thermal resistivity (see Refs. [14, 17, 19, 20] for thorough explanations). These processes can, however, affect the thermal conductivity indirectly, enhancing or modifying the effect of other scattering mechanisms, i.e. the phonon-imperfection scattering (see discussion of some examples in Refs. [14, 20]). In contrast to *N*-processes, the large changes in crystal momentum in *U*-processes make it possible for them to be an effective source of thermal resistivity. The probability of *U*-processes is, however, temperature dependent, so that they play a dominant part at high temperatures ( $T \gtrsim \Theta_D$ ), but are of little

importance at low temperatures ( $T \ll \Theta_D$ ), where only  $N$ -processes can occur at an appreciable rate. The reason is that at any temperature  $T$ , only the so called, thermal or dominant phonons with energy  $\hbar\omega \simeq k_B T$  are present in an appreciable number and can, therefore, be involved significantly in different interactions with other quasiparticles (phonons included). The wave length,  $\lambda_p$ , and modulus,  $q_T$ , of the wave vector of thermal phonons are given by

$$\lambda_p = 2\pi \frac{\hbar v_s}{k_B T}, \quad (9)$$

and

$$q_T = \frac{k_B T}{\hbar v_s} = \left( \frac{T}{\Theta_D} \right) q_D, \quad (10)$$

where  $q_D$  is the Debye wave vector.

It can be seen from Eqs. (8) that to ensure an  $U$ -process, some of the participating phonons should have a large enough wave vector, at least  $q \simeq (1/2)g$  according to [17], (i. e., comparable with  $q_D$ ) and high enough energy (comparable with  $k_B \Theta_D$ ). Thus, the  $U$ -processes can have an appreciable rate only at temperatures in the vicinity of or above  $\Theta_D$ .

Now consider the temperature dependence of the thermal conductivity,  $\kappa(T)$ , of a rather perfect non-metallic crystal. At sufficiently high temperatures ( $T > \Theta_D$ ), the specific heat of the crystal should be constant [Eq. (6b)], and, therefore, the temperature dependence  $\kappa(T)$  is determined solely by that of the phonon-phonon scattering rate,  $\tau_{pp}^{-1}$ . The dominant contribution to the thermal resistivity in this temperature range is from  $U$ -processes. The rate,  $\tau_{pp}^{-1}$ , should increase with temperature, since the total number of phonons (which are scatterers to other phonons which carry heat) is proportional to  $T$  in this temperature range. It is expected [14, 17, 19, 20] that  $\tau_{pp}^{-1} \propto T^n$  with  $n = 1$  for the three-phonon processes, which is to say that  $\kappa_p \propto 1/T$ . More elaborate theoretical calculations [17, 20] give

$$\kappa_p \propto \frac{a M_a \Theta_D^3}{T \gamma_G^2}, \quad (11)$$

where  $a^3$  gives the volume occupied by one atom,  $M_a$  is the atomic weight,  $\gamma_G$  is Grüneisen constant. The  $1/T$  law can be considered as a good approximation for the lattice thermal conductivity of fairly perfect crystals at  $T > \Theta_D$  [20].

For  $T < \Theta_D$ , the probability of  $U$ -processes drops sharply as temperature decreases. In this temperature range theoretical calculations give  $\tau_{pp} \propto \exp(\Theta_D/bT)$  and

$$\kappa_p \propto T^x \exp(\Theta_D/bT), \quad (12)$$

with  $x$  and  $b$  both of the order of unity [17, 19, 20]. In this case the relaxation time  $\tau_{pp}$  and thermal conductivity increase exponentially with decreasing temperature. This increase

lasts until the phonon-phonon mean free path,  $l_{pp} = v_s \tau_{pp}$ , becomes comparable with that of the phonon-imperfection scattering or even with dimensions of the sample (boundary scattering). In this case the effective time of phonon relaxation becomes temperature independent, and the temperature dependence of  $\kappa_p$  will be determined by that of the specific heat, which reduces with temperature as  $T^3$  for  $T \ll \Theta_D$ .

In summary, the  $\kappa_p(T)$  dependence for fairly perfect non-metallic crystals behaves as follows. At high temperatures  $T > \Theta_D$ , it is proportional to  $1/T$  ( $1/T$  law). As temperature decreases below  $\Theta_D$ ,  $\kappa_p(T)$  increases exponentially according to Eq. (12) reaching a maximum at a temperature, at which the phonon mean free path begins to be determined by imperfections or outer boundaries of the sample. With decreasing temperature, the mean free path becomes temperature independent, and, therefore, the temperature dependence of  $\kappa_p$  is determined by that of the specific heat, which is proportional to  $T^3$  for  $T \ll \Theta_D$ .

A clear manifestation of this exponential law [Eq. (12)] is confined to range  $1/30 < T/\Theta_D < 1/10$  [20]. This sets an upper temperature limit for the position of the thermal conductivity peak. The peak can be seen, however, only in rather pure and perfect non-metallic crystals. Crystal-lattice imperfections (lattice defects) are effective phonon scatterers. They cause an extra thermal resistance which can even suppress the thermal conductivity peak completely. Although rather considerable theoretical and experimental efforts were made to resolve this problem (see [17, 20] and references therein), the understanding level achieved only allows some general discussion and speculation regarding analysis of imperfection effects in experimental thermal conductivity data.

The important feature of lattice defects is whether their linear dimensions are larger or smaller than the phonon wavelength. The first type of defects include, for example, external or internal (grain) boundaries, dislocations, stacking faults. The second type is represented mainly by point defects or small precipitate particles due to phase inhomogeneity. It is obvious that some defects can change their type with changing temperature since the wavelength,  $\lambda_p$ , of dominant phonons depends on temperature as  $1/T$  [Eq. (9)]. It can encompass hundreds of interatomic distances for  $T \ll \Theta_D$ ; whereas, it is of the order of the interatomic distance at  $T \geq \Theta_D$ . This is in sharp contrast with the wavelength of electrons in good metals, which is always of the order of the interatomic distance, independent of temperature.

Among other imperfections, the point defects are considered as the most important source of thermal resistance. These are impurity atoms, isotopes, lattice vacancies and interstitial atoms. The point defects introduce small perturbations of mass, force constant and nearest-neighbor distance, causing elastic phonon scattering. Their size is of order

of the interatomic distance. The known theoretical results [17, 20] give, in most cases, only general ideas about the influence of point defects on the thermal conductivity. At low temperature  $T \ll \Theta_D$  (when  $\lambda_p$  is well over the size of point defects) the mechanism of phonon-point defect relaxation is thought to be similar to that of Rayleigh scattering, for which the relaxation rate is proportional to  $\omega^4$  [17, 20]. Since  $\omega \approx k_B T / \hbar$  for dominant phonons, the relation,  $\tau_{pi}^{-1} \propto T^4$ , should hold for the rate of phonon-point defect relaxation. In this case, for the low temperature range where phonon specific heat is proportional to  $T^3$ , the thermal conductivity should be proportional to  $1/T$ . If phonon-point defect scattering is dominant at low temperatures, the exponential rise in thermal conductivity due to  $U$ -processes [Eq. (12)] will be suppressed. At temperatures so low that the phonon mean free path,  $l_{pi} = v_s \tau_{pi}$ , associated with phonon-point defect scattering, becomes comparable with the sample dimensions and, hence, temperature independent, the thermal conductivity goes to zero with decreasing temperature according to relation  $\kappa_p \propto T^3$ .

As temperature increases, the phonon wavelength,  $\lambda_p$ , decreases, approaching an interatomic distance. This causes the rate of phonon-point defect relaxation to become temperature independent. At high enough temperature this is true for phonon relaxation by any lattice defects, regardless of the temperature scattering law for the defects at low temperature [20]. It follows from the aforesaid that the phonon-point defect contribution to thermal resistivity can be appreciable at high temperatures ( $T \gtrsim \Theta_D$ ), where it depends only slightly on temperature, while at low enough temperatures the phonon wavelength becomes so long that scattering by point defects (and by most of the other lattice defects) becomes negligible. It should be recalled that the electron wavelength in good metals is always of the order of the interatomic distance, and electron-imperfection scattering is temperature independent. For this reason, imperfections remain the only source of electron scattering for temperatures so low that the electron-phonon relaxation processes are essentially frozen out. This important difference in the behaviors of electrons and phonons, as heat carriers, should be taken into account in consideration of the electron and phonon contributions to thermal resistance at low temperatures.

In conductors with a fairly high free electron concentration, the phonon-electron scattering [see Eq. (7)] can give an appreciable contribution to thermal resistance. This problem is, however, so closely connected with electrical and thermal conductivities of electrons that it is appropriate to consider it after the main concepts of the electronic thermal conductivity will be discussed in the next section.

## B. Electronic thermal conductivity

For considerations of electronic thermal conductivity, the general expression given by Eq. (2) is used, taking  $C_v$  to be the electronic specific heat  $C_e$  and  $\bar{v}$  is the Fermi velocity  $v_F$ , i. e.

$$\kappa_e(T) = \frac{1}{3}C_e v_F l = \frac{1}{3}C_e v_F^2 \tau. \quad (13)$$

The electronic specific heat in the free-electron model [17–19] is given by

$$C_e = \frac{\pi^2}{2} \left( \frac{k_B T}{\mathcal{E}_F} \right) n_e k_B = \gamma T, \quad (14)$$

where  $\mathcal{E}_F$  is the Fermi energy,  $n_e$  is electronic density, and  $\gamma$  is the Sommerfeld coefficient. The linear dependence on temperature is quite general, however, and holds for any Fermi liquid, independent of the free-electron model.

It is of fundamental importance that the same scatterers (phonons and lattice defects) determine the resistance to both the charge and the heat transport of electrons. The electronic conductivity,  $\sigma$ , in the frame of free-electron model is given by [17–19]

$$\sigma = \frac{n_e e^2 \tau}{m}. \quad (15)$$

When expressions for electronic thermal and electrical conductivities [Eqs. (13) and Eq. (15)] are compared to one another, it is apparent (using Eq. (14) for electronic specific heat as well) that  $\kappa_e/(\sigma T)$  should be constant, if the electron relaxation times (the total relaxation time,  $\tau$ ) are equal for both kinds of electron transport. This simple relation is the famous Wiedemann-Franz (WF) law. In the free-electron model this law is expressed as [17–19]

$$\frac{\kappa_e}{\sigma T} = L_0, \quad (16)$$

where  $L_0 = (\pi^2/3) (k_B/e)^2$  is called the Lorenz number.

The WF law forms the basis for separation of the electron and phonon contributions to thermal resistance during analysis of experimental data on thermal conductivity. This law appears, however, to be true only at the lowest temperatures, where electron-imperfection scattering is dominant, and at high temperatures ( $T/\Theta_D \gtrsim 1$ ). In the intermediate temperature range, a significant violation of the WF law takes place. The reason is that the electrical and thermal conductivities are determined by different types of electron-phonon collisions in this intermediate temperature range. To make this point more clear, let us write in the Matthiessen's approximation the more detailed expressions for the thermal and electrical resistivities:

$$1/\kappa_e = W_e = W_{ep} + W_{ei} = \frac{3}{C_e v_F^2} [\tau_{ei}^{-1} + \tau_{ep(\kappa)}^{-1}(T)], \quad (17)$$

$$\rho = \rho_{\text{ep}} + \rho_{\text{ei}} = \frac{m}{n_e e^2} [\tau_{\text{ei}}^{-1} + \tau_{\text{ep}(\sigma)}^{-1}(T)], \quad (18)$$

where subscript **ei** indicates the electron-imperfection interaction (which is temperature independent), and subscripts **ep**( $\kappa$ ) and **ep**( $\sigma$ ) indicate electron-phonon interactions, crucial for thermal and electrical conductivities, respectively. Of course, some other sources of electron scattering can be indicated as well (for example, electron-electron scattering or the spin disorder in paramagnetic, ferromagnetic or antiferromagnetic states), but the two mentioned above are considered as the most significant.

The times  $\tau_{\text{ep}(\sigma)}$  and  $\tau_{\text{ep}(\kappa)}$  are characterized by the following temperature behaviors [17–19]:

$$\tau_{\text{ep}(\sigma)}^{-1}(T) \propto \begin{cases} T^5 & \text{if } T \ll \Theta_D, \\ T & \text{if } T \gtrsim \Theta_D; \end{cases} \quad (19)$$

$$\tau_{\text{ep}(\kappa)}^{-1}(T) \propto \begin{cases} T^3 & \text{if } T \ll \Theta_D, \\ T & \text{if } T \gtrsim \Theta_D. \end{cases} \quad (20)$$

It is seen that temperature dependences of these times are the same near or above  $\Theta_D$ , but are quite different below it. Consider briefly the sources of this diversity. When an electron with wave vector  $\mathbf{k}$  is scattered by a phonon into the state  $\mathbf{k}'$ , the electron either absorbs or emits a phonon of wave vector  $\mathbf{q}$ . These collisions are determined by the following rules [17–19]:

$$\mathbf{k}' = \mathbf{k} \pm \mathbf{q} + \mathbf{g}, \quad (21a)$$

$$\mathcal{E}_{\mathbf{k}'} = \mathcal{E}_{\mathbf{k}} \pm \hbar\omega_{\mathbf{q}}. \quad (21b)$$

The first rule maintains that momentum is conserved, up to the addition of any arbitrary vector of the reciprocal lattice. In the same way as for the phonon-phonon scattering (see Sec. III A), the cases  $\mathbf{g} = 0$  and  $\mathbf{g} \neq 0$  correspond to *N*- and *U*-processes, respectively. It should be noted that the *U*-processes of the electron-phonon interaction are very improbable at low temperature, but they can increase somewhat the electronic electrical and thermal resistivities at fairly high temperatures (above  $\approx 0.2 \Theta_D$ ). The second rule is the requirement for conservation of energy in the interaction.

The maximum phonon energy is about  $k_B \Theta_D$ , which is much less than the electron energy,  $\mathcal{E}_F$ . For this reason, the electron-phonon collisions could be considered as quasi-elastic ones. For electronic thermal conduction, however, it is more important to compare the change in electron energy in a collision ( $\Delta \mathcal{E}_{\mathbf{q}} = |\mathcal{E}_{\mathbf{k}} - \mathcal{E}_{\mathbf{k}'}|$ ) with  $k_B T$  (since electrons in metals can change their energy only in narrow band near the Fermi level with a width about  $k_B T$ ). Following this criterion, the collisions with  $\Delta \mathcal{E}_{\mathbf{q}} \simeq k_B T$  are considered

as inelastic ones while those with  $\Delta\mathcal{E}_{\mathbf{q}} < k_{\text{B}}T$ , as elastic [17–19]. These collisions are quite effective for electronic thermal resistance. At low temperatures,  $T \ll \Theta_{\text{D}}$ , they are inelastic (since the energy of the dominant phonon is about  $k_{\text{B}}T$  in this temperature range) with a collision rate (or an inverse relaxation time,  $1/\tau_{\text{ep}}$ ) proportional to  $T^3$  [17, 19]. This corresponds to the low temperature behavior of time  $\tau_{\text{ep}(\kappa)}$  in Eq. (20), governing the electronic thermal resistance.

At low temperatures,  $T \ll \Theta_{\text{D}}$ , a single collision, which must be an  $N$ -process according to the selection of Eq. (21), is, however, ineffective in providing electrical resistance. The reason is that the electron direction of motion can be changed only slightly in this  $N$ -process. The angle between vectors  $\mathbf{k}$  and  $\mathbf{k}'$  (the angle of scattering) is  $\theta \simeq q_{\text{T}}/k_{\text{F}} = T/\Theta_{\text{D}}$ , that is, very small. An electron must endure many of such collisions to gain a large scattering angle, and the probability of that event is proportional to  $(T/\Theta_{\text{D}})^2$  [17–19]. For this reason, the effective rate of the electron-phonon relaxation for electrical resistance is  $\tau_{\text{ep}(\sigma)}^{-1}(T) \propto T^3(T/\Theta_{\text{D}})^2 \propto T^5$ , which was already indicated in Eq. (19).

At high temperatures,  $T > \Theta_{\text{D}}$ , any electron-phonon collision is large-angle and elastic. Since the total number of phonons is proportional to  $T$  at this temperature range, the relation  $\tau_{\text{ep}}^{-1} \propto T$  holds for both electron charge and heat transport.

We can survey now a temperature dependence of the electronic thermal conductivity, taking into account Eqs. (13), (14) and (17). At temperatures so low that the elastic and temperature independent electron-imperfection scattering is dominant, the thermal conductivity behaves as  $\kappa_{\text{e}}(T) \propto T$ . In this temperature range the WF law [Eq. (16)] holds. For higher temperatures, the electron-phonon scattering becomes dominant. At  $T \ll \Theta_{\text{D}}$ , this scattering is inelastic with rate,  $\tau_{\text{ep}(\kappa)}^{-1} \propto T^3$ , relevant for heat transport, and the rate  $\tau_{\text{ep}(\sigma)}^{-1} \propto T^5$ , relevant for charge transport. This leads to the relation  $\kappa_{\text{e}}(T) \propto T^{-2}$ . Due to different electron-phonon relaxation rates, relevant for charge and heat transport, the WF law is not obeyed in this temperature range, so that the ratio  $\kappa_{\text{e}}/(\sigma T)$  is not constant, but is proportional to  $T^2$ . At high temperatures,  $T > \Theta_{\text{D}}$ , electron-phonon collisions are elastic with rate  $\tau_{\text{ep}}^{-1} \propto T$ , which gives relations,  $\rho \propto T$ , for electrical resistivity and,  $\kappa_{\text{e}}(T) = \text{const}$ , for thermal conductivity. The WF law holds in this temperature range. For fairly perfect metals with high electron density, the electron contribution dominates in thermal conductivity, so that the outlined features of  $\kappa_{\text{e}}(T)$  dependence are immediately evident from measured  $\kappa(T)$  curves. An example of such behavior is presented in Fig. 1 for a well annealed silver foil [16].

It is seen that a concurrence of the electron-imperfection and electron-phonon interactions gives rise to a maximum (a peak) in the  $\kappa_{\text{e}}(T)$  dependence. This peak can be very sharp for fairly perfect and pure metals, where the peak position,  $T_{\text{max}}$ , is usually below

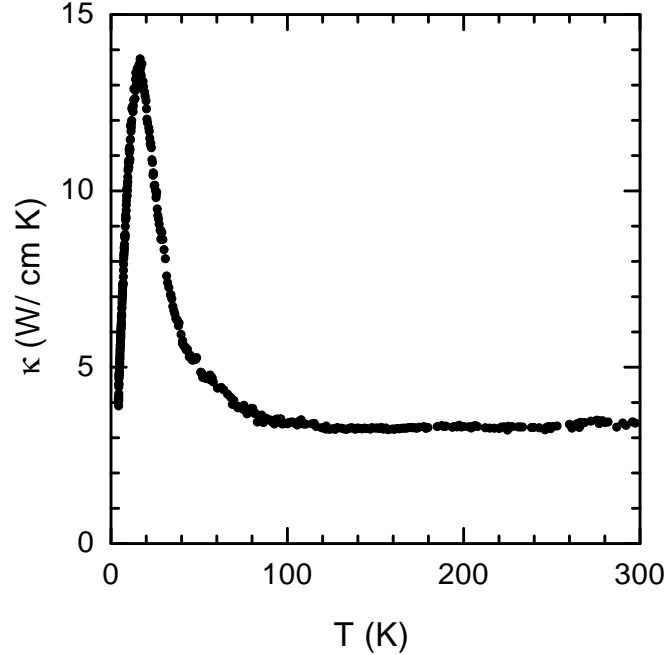


FIG. 1:  $\kappa_e(T)$  dependence of annealed silver foil.

$0.1 \Theta_D$ . Lattice defects induce the following: (i) an increase in slope of the linear part of  $\kappa_e(T)$  dependence; (ii) an increase in  $T_{\max}$ ; and (iii) a decrease in the peak height up to a total smearing of it for strong enough lattice disorder. Some clear demonstrations of this imperfection effect for typical metals can be found in [14, 15, 18, 20, 28]. It is apparent also [see Eq. (17)] that in “bad” metals with strong electron-imperfection scattering the WF law is obeyed better (even in the intermediate temperature range where inelastic electron-phonon scattering occurs) than in pure metals with a perfect crystal lattice.

### C. Effects of phonon-electron interactions in thermal conductivity

The phonon-electron scattering can limit the phonon thermal conductivity (this point was briefly mentioned at the end of Sec. III A). This interaction leads to absorption or emission of phonons by electrons and is restricted by the above-mentioned rules for electron-phonon interaction [Eq. (21)]. The thermal resistivity, determined by these processes, is labelled  $W_{pe}$  in the general expression (7) for phonon thermal resistivity with an associated relaxation time  $\tau_{pe}$ . The known theoretical examinations [14, 17, 20] have shown that  $\tau_{pe}^{-1}(T) \propto T$  if  $T \ll \Theta_D$ , and is constant if  $T > \Theta_D$ . This leads [taking into

account Eqs. (6) and (7)] to

$$W_{\text{pe}} \propto \begin{cases} T^{-2} & \text{if } T \ll \Theta_{\text{D}}, \\ \text{const} & \text{if } T > \Theta_{\text{D}}. \end{cases} \quad (22)$$

Equations (22) actually results from the more general relation [17]

$$\frac{W_{\text{pe}}T}{\rho} \leq \left(\frac{e}{k_{\text{B}}}\right)^2 n_{\text{a}}^2 \left(\frac{3Nk_{\text{B}}}{C_{\text{p}}}\right)^2, \quad (23)$$

where  $n_{\text{a}}$  is the number of conduction electrons per atom. Besides the electron-phonon  $N$ -processes, this equation takes into account the  $U$ -processes as well, and that causes an appearance of the nonequality sign. It is easy to verify that in the case of the equality sign (that is, ignoring the  $U$ -processes) the relationships (22) can be derived from Eq. (23) for low ( $T \ll \Theta_{\text{D}}$ ) as well as for high ( $T > \Theta_{\text{D}}$ ) temperatures. In the former case, the relationships  $\rho \propto T^5$  and  $C_{\text{p}} \propto T^3$  should be taken, and in the latter case,  $\rho \propto T$  and  $C_{\text{p}} = 3Nk_{\text{B}}$ .

Equation (23) has a doubtless similarity with the WF law presented by Eq. (16). At high temperatures ( $C_{\text{p}} = 3Nk_{\text{B}}$ ) it is possible to rewrite it as

$$\frac{\rho}{W_{\text{pe}}T} = \frac{\kappa_{\text{pe}}}{\sigma T} \geq \left(\frac{k_{\text{B}}}{e}\right)^2 \frac{1}{n_{\text{a}}^2}. \quad (24)$$

The right-hand side of the equation is quite close to the Lorenz number,  $L_0 = (\pi^2/3)(k_{\text{B}}/e)^2$ . This implies that the phonon thermal conduction at high temperatures is comparable with the electronic thermal conduction, if both of them are determined by the electron-phonon scattering only [17].

#### D. Superconductivity effects in thermal conductivity

In superconductors, as temperature crosses  $T_{\text{C}}$  from above, some number of electrons,  $n_{\text{s}}$ , becomes superconducting, while the rest of them, in number  $n_{\text{n}}$ , would remain as before in the normal state. The fraction of superconducting electrons [given by  $x = n_{\text{s}}/(n_{\text{s}} + n_{\text{n}})$ ] increases continuously with decreasing temperature from  $x = 0$  at  $T = T_{\text{C}}$  to  $x = 1$  at  $T = 0$ . The superconducting electrons are in a bound state (Cooper pairs), in which they are unable to transport entropy or interact with phonons. But the rest of the electrons (the fraction,  $1 - x$ ) being normal, remain heat carriers and can interact with the phonons.

Even in the frame of this simple picture (which is in the spirit of the two-fluid model of Gorter and Casimir) some quite definite predictions about the effects of superconductivity

on the thermal conductivity can be made. Before doing this, let us denote the electronic thermal conductivity in the superconducting state as  $\kappa_e^s$ , and that in the normal state (induced, for example, by high enough magnetic field) as  $\kappa_e^n$ . The same kind of notations ( $\kappa_p^s$  and  $\kappa_p^n$ ) will be used in the following for the phonon part of the thermal conductivity or even for the total thermal conductivity ( $\kappa^s$  and  $\kappa^n$ ). It is clear that the ratio  $\kappa_e^s/\kappa_e^n$  must reduce continuously with decreasing temperature below  $T_C$  from the initial value (equal to unity) at  $T = T_C$  to values much less than unity at low enough temperature. All this takes place due to a decrease in the fraction of the normal electrons when going below  $T_C$ . The same reason (that is a decrease in the number of the normal electrons below  $T_C$ ) can, however, induce an increase in the ratio,  $\kappa_p^s/\kappa_p^n$ , for the phonon contribution, causing it grow far above unity with decreasing temperature in the range not too far below  $T_C$ . In this case a reduction in the number of normal electrons (which are the main phonon scatterers in metals for low temperatures) can cause a decrease in the phonon-electron relaxation rate,  $1/\tau_{pe}$ , and, hence, an increase in the phonon thermal conductivity (it follows from Eq. (23) that  $\kappa_{pe} \propto 1/n_e$ ).

The basic theoretical results on the superconductivity effects in the thermal conductivity were obtained mainly in the frame of the BCS model [21–27]. Consider them separately for the electron and phonon contributions to the thermal conductivity. It turns out to be rather important for the electron heat transport whether the critical temperature  $T_C$  falls below or above the peak in the temperature dependence of  $\kappa_e(T)$ . In the former case, the normal electrons (or as it is often said, quasiparticle excitations) are scattered predominantly by the lattice imperfections, while in the latter case, by phonons. For both cases rather cumbersome expressions for temperature dependences of  $\kappa_e^s/\kappa_e^n$  were derived which can be found in Refs. [1, 21–27]. We shall restrict ourselves to consideration of the graphical representations of these dependences shown in Fig. 2(a). When defects are the dominant electron scatterers, the function  $\kappa_e^s/\kappa_e^n = f(T)$  has a zero slope at  $T_C$  [solid curve in Fig. 2(a)]; whereas, in the case that electrons are scattered mainly by phonons [dashed curve in Fig. 2(a)], the slope at  $T_C$  is rather large (about 1.62 according to Ref. [24]). Theories [21–27], including the so called BRT model [22, 24, 26], agree well with experiment for the case of predominantly electron-imperfection scattering that is found for pure low- $T_C$  superconductors with high electron density like Al, In, Sn and some others (see [14, 24, 27]). For the case where electron-phonon scattering dominates, the agreement between theory and experiment is not so convincing.

It should be noted that for a comparison between the theories [21–25] and experimental data one must know exactly the “normal” behavior of thermal conductivity below  $T_C$  since a theoretical expression for  $\kappa_e^s/\kappa_e^n = f(T)$  is used for the comparison. For a weak

superconductor with low  $T_C$ , the “normal” thermal conductivity can be measured below  $T_C$  under a magnetic field which is high enough to suppress superconductivity. This is not feasible, however, for superconductors (like cuprates) with high  $T_C$  and huge critical magnetic fields. Besides, when  $T_C$  is high enough (as in the cuprates) and falls into the temperature range where electron-phonon scattering dominates, the WF law fails and does not give a good estimate of the electronic part of the thermal conductivity from the total measured thermal conductivity (see Sec. IIIB). The comparison with BRT and other models in the case of superconductors with high enough  $T_C$  poses, therefore, great difficulties.

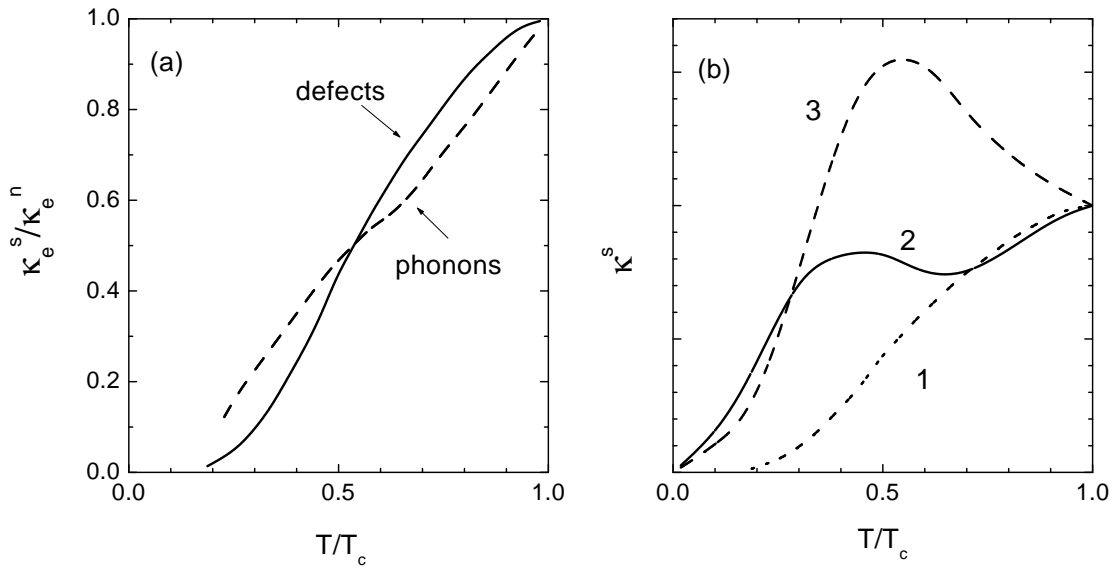


FIG. 2: Left panel (a) presents theoretical temperature dependences of the ratio of electronic thermal conductivities in superconducting and normal states,  $\kappa_e^s/\kappa_e^n$ , below  $T_C$  for the cases when the electrons are scattered predominantly by defects (solid line) or by phonons (dashed line) [21–25]. Right panel (b) presents schematic sketches of temperature dependences of the total thermal conductivity below  $T_C$  for different relationships between the electron and phonon contributions to the thermal conductivity. Expected behaviors for the cases when the electrons or phonons dominate the thermal conductivity are presented by curves 1 (dotted line) and 3 (dashed line), respectively. Curve 2 (solid line) presents the intermediate case when both kinds of the heat carriers compete on equal terms in the thermal conductivity.

The phonon contribution to heat transport can be quite appreciable for some materials and be comparable or even higher than that of the electrons. In this case the thermal con-

ductivity behavior below  $T_C$  can be partially or totally determined by phonon transport. Figure 2(b) presents schematic sketches of possible temperature dependences of the total thermal conductivity,  $\kappa^s$ , below  $T_C$  for different relationships between the electron and phonon contributions to the thermal conductivity. A behavior of  $\kappa^s(T)$  for a limiting case when the electron contribution dominates is presented by curve 1 (dotted line). This type of behavior is expected for rather perfect superconducting metals with a high electron concentration. Another limiting case, when phonons dominate in the thermal conductivity, is illustrated by curve 3 (dashed line). In this case (as was already mentioned above), the phonon thermal conductivity increases below  $T_C$  with decreasing temperature due to the decrease in the number of normal electrons with a corresponding decrease in the phonon-electron relaxation rate. At low enough temperature the phonons begin to be scattered primarily by crystal boundaries, so that the phonon mean free path becomes temperature independent. After that, according to general relation (2),  $\kappa^s(T)$  decreases to zero with decreasing temperature with the resulting formation of a maximum in  $\kappa^s(T)$  dependence [curve 3 in Fig. 2(b)]. This type of the  $\kappa^s(T)$ -behavior is expected in disordered metals and alloys with high electron-imperfection scattering (that depresses the electron contribution to the thermal conductivity), and was seen in some disordered low- $T_C$  superconductors [25, 29]. This behavior was found to be in good agreement with the theory of Geilikman and Kresin [25]. The phonon thermal conductivity may be dominant also in rather perfect metals which have a low free electron density. This is characteristic of high- $T_C$  cuprates where  $\kappa^s(T)$ -behavior, similar to that of curve 3 in Fig. 2(b), is frequently observed [1].

The curves 1 and 3 in Fig. 2(b) present the limiting cases when one type of heat carriers (electrons or phonons) dominates the thermal conductivity. It is apparent that, for many materials, the electron and phonon contributions will be of the same order. This will lead to dependences which are intermediate between the two limiting cases. Curve 2 (solid line) in Fig. 2(b) presents one of the possible intermediate cases when both kinds of the heat carriers compete on equal terms in the thermal conductivity. Some examples of this kind of  $\kappa^s(T)$  behavior for low- $T_C$  superconductors can be found in Ref. [25].

## IV. RESULTS AND DISCUSSION FOR MAGNETIC SUPERCONDUCTORS

### A. Rare-earth Nickel Borocarbides

In this section we consider the thermal conductivity data for rare-earth nickel borocarbides,  $RNi_2B_2C$ , with  $R = Y, Lu, Yb, Tm, Er, Ho, Dy, Tb$  or  $Gd$  (which will be referred

below to as borocarbides). Although only those members with  $R = \text{Tm, Er, Ho and Dy}$  are magnetic superconductors, for the sake of completeness and to illustrate similarities for the members that exhibit only one of these behaviors (only superconductivity, only magnetism) or even neither, all members will be discussed. Before going directly to this matter, it is appropriate first to briefly review the basic properties of these compounds. For extended reviews of experimental and theoretical findings for borocarbides see Refs. [30–33].

### 1. General Properties

The crystal structure of  $\text{RNi}_2\text{B}_2\text{C}$  is a body-centered tetragonal with space group  $I4/mmm$  [34]. It is a layered structure in which  $\text{Ni}_2\text{B}_2$  layers are separated by R-C planes stacked along the  $c$ -axis. The Ni atoms are tetrahedrally coordinated to four B atoms. Despite the layered structure, the electronic properties of borocarbides appear to be essentially three-dimensional according to electronic band structure calculations [35], supported by the spectroscopic studies [36]. These compounds are rather good metals with a large electron density of states  $N(\mathcal{E}_F)$  at the Fermi level. The dominant contribution to  $N(\mathcal{E}_F)$  comes from Ni  $3d$ -states, but some contributions come from all other atoms as well [35]. Resistivity and magnetoresistance of  $\text{RNi}_2\text{B}_2\text{C}$  borocarbides ( $R = \text{Y, Lu, Er, Ho}$ ) [37] have not revealed appreciable anisotropy between measurements normal to the  $ab$ -plane (along the  $c$ -axis) and in-plane, consistent with the three-dimensional character of the electronic properties. Small deviations from isotropic behavior were observed below 150 K for the compounds containing magnetic ions (Er and Ho), which was attributed in Ref. [37] to crystal-electric field effects.

Among the  $\text{RNi}_2\text{B}_2\text{C}$  family, the compounds with  $R = \text{Y, Lu, Yb}$  are non-magnetic (the last is a heavy-fermion system), but all others ( $R = \text{Gd, Tb, Dy, Ho, Er, and Tm}$ ) are magnetic. Their magnetic properties are determined by the localized electrons in the  $4f$ -shell of R atoms. Long range magnetic order is due to the indirect RKKY interaction, mediated through the conduction electrons. This gives rise to different types of antiferromagnetic (AFM) order of the  $4f$ -ions [38]. Borocarbides with  $R = \text{Tm, Er, Ho, Dy}$  show coexistence of superconductivity and magnetic order. More information about superconducting and magnetic properties of these compounds can be found in Table I.

A Cooper pair consists of two electrons with equal and opposite moment, and with opposite spins (the total momentum and spin of the pair are zero). Any perturbation which acts with opposite signs (or with opposing force) on the two members of a Cooper pair can destroy this pair, producing a, so called, pair breaking effect. For example,

TABLE I: Low temperature phase states of the  $RNi_2B_2C$  bulk compounds (taken from Refs. [31, 33, 38] unless otherwise referenced).  $R = Y$  or rare-earth element,  $T_C$  is the superconducting transition temperature,  $T_M$  is the magnetic transition temperature,  $T_K$  is Kondo temperature. Column “Magnetic Transition” indicates magnetic states into which the compounds can be transformed (AFM = antiferromagnet, MAFM = modulated incommensurate antiferromagnet and WFM = weak ferromagnet),  $\vec{q}$  is the wave vector of the modulated magnetization (in units of reciprocal lattice parameters) and the symbol  $\uparrow\parallel$  indicates magnetic moment directions. Abbreviation HFS denotes heavy-fermion system.

R	$T_C$ (K)	$T_M$ (K)	Magnetic Transition
Y	15.7	0	none
Lu	16.6	0	none
Yb	<0.05	<0.023 [39]	HFS, $T_K = 10$ K, $\gamma = 530$ mJ/mol-K
Tm	11	1.5	MAFM $\vec{q} \approx 0.094(a^* \pm b^*) \uparrow\parallel <001>$
Er	11	6.8	MAFM $\vec{q} \approx 0.55a^* \uparrow\parallel <010>$
		2.3	WFM $\uparrow\parallel <100>$ or $<110>$ [40]
Ho	8.5	6.0	MAFM $\vec{q} \approx 0.585a^*, 0.915c^*$
		5.5	MAFM $\vec{q} \approx ?$
		5.2	AFM $\vec{q} = c^* \uparrow\parallel <110>$
Dy	6.2	10.3	AFM $\vec{q} = c^* \uparrow\parallel <110>$
Tb	<0.3	14	MAFM $\vec{q} \approx 0.55a^* \uparrow\parallel <100>$
		6-8	WFM $\uparrow\parallel <100>$ or $<110>$ [41]
Gd	<0.3	20	MAFM $\vec{q} \approx 0.55a^* \uparrow\parallel <010>$
		13.6	Tilted MAFM

an external or the internal (in magnetic materials) magnetic field exerts an orbital pair-breaking effect since the field acts with opposing force on the two electron momenta in the pair. If some ions in a metal system have a magnetic moment, ion spins will act with opposite sign on the electron spins in the pair (the magnetic pair-breaking). Generally speaking [42], such types of perturbations lead to breaking of the time-reversal properties of the system and, hence, can cause a strong decrease in  $T_C$  or even total suppression of superconductivity.

In the case of rare-earth compounds, localized  $4f$ -electrons should undoubtedly exert a pair-breaking effect on the superconductivity. Since, however, the  $4f$ -electrons are

strongly localized in deep inner  $4f$ -orbitals, their interaction with conducting electrons can be rather weak, thus, permitting coexistence of superconductivity and the long range magnetic order. Such a situation is believed to take place for rare-earth rhodium boride compounds, Chevrel phases [5–7], and borocarbides [30]. Coexistence of superconductivity and AFM order was justified theoretically rather long ago [43]. The coexistence is possible if the AFM exchange field averages to zero within the superconducting coherence length,  $\xi$ . AFM order is, however, expected to have a profound effect on superconducting and transport properties, and this was found in the above-mentioned magnetic superconductors.

The theoretical and experimental studies generally indicate that the borocarbides are conventional electron-phonon mediated superconductors with  $s$ -wave symmetry for the order parameter [30, 36]. On the other hand, some members of the borocarbide family manifest properties which are suggestive of unconventional or exotic superconductors [32, 44–46]. In spite of this, the borocarbides are reasonably considered to be conventional superconductors.

Rare-earth borocarbides are rather good conductors, comparable to transition metals or their alloys. They have high electron density. According to Ref. [47], the value of  $n_e$  for Y-, Ho-, and Gd-based borocarbides are 2.63, 3.12 and  $5 \times 10^{22} \text{ cm}^{-3}$ , respectively. These values are only moderately less than those of simple superconducting metals, such as Al, Pb or Sn [19]. The Fermi velocity values,  $3.6 \times 10^7 \text{ cm/s}$  (calculated for  $\text{LuNi}_2\text{B}_2\text{C}$  by Pickett and Singh [35]), and  $4.2 \times 10^7 \text{ cm/s}$  (found by de Haas-van Alphen studies in  $\text{YNi}_2\text{B}_2\text{C}$  [48]) are, however, clearly much less than the typical value  $v_F \approx 2 \times 10^8 \text{ cm/s}$  for simple metals [19]. Measurements of transport properties of borocarbide single crystals [31, 37, 49] have shown that the resistivity at room temperature,  $\rho_{\text{RT}}$ , is typically in the range 35–70  $\mu\Omega \text{ cm}$ , and that the residual resistivity,  $\rho_0$ , is in the range 2–5  $\mu\Omega \text{ cm}$  ( $T < 10 - 15 \text{ K}$ ), so that the ratio  $\rho_{\text{RT}}/\rho_0$  is in the range 10–30. These conducting properties, though rather good, are not so good as those of the pure simple metals, for which  $\rho_0$  can be as low as 0.01  $\mu\Omega \text{ cm}$  and  $\rho_{\text{RT}}/\rho_0$  can be as high as a thousand [50]. It thus follows that the relative electron contribution to the total thermal conductivity in borocarbides should be much less than that in pure simple metals. For this reason, some manifestations of the phonon contribution in the behavior of the total thermal conductivity of borocarbides is expected. In particular, due to the rather high residual resistivity,  $\rho_0$ , the phonon effects may show themselves below  $T_C$ . The high  $\rho_0$ -values even in single-crystals are possibly determined by some types of inhomogeneities and point defects. The known studies [51] suggest vacancies at the boron/carbon sites, which have no appreciable influence on bulk superconducting properties. The vacancies can raise,

however,  $\rho_0$ -values considerably, depressing in this way the electronic thermal conductivity and enhancing the role of the phonon thermal conductivity in the low temperature range.

The temperature dependence of the resistivity in borocarbides deserves some attention since it may be important for consideration of their thermal conductivity. The experimental  $\rho(T)$  curves are found to be approximately linear in the range 100–300 K (see  $\rho(T)$  plot for  $\text{LuNi}_2\text{B}_2\text{C}$  in Fig. 17) [31, 49]. Below 50 K,  $\rho(T)$  is essentially non-linear and, in a rather narrow range  $1.25 T_C < T < (30-40)$  K, can be approximated by  $\rho(T) = \rho_0 + aT^p$ , where  $p$ -values for  $\text{RNi}_2\text{B}_2\text{C}$  compounds are in the range  $2.0 \lesssim p \lesssim 2.6$  [31, 49].

Since the specific heat enters the general expression (2) for the thermal conductivity, a brief mention should be made of this point. Most studies focussed on the specific heat in the neighborhood of  $T_C$  (above and below it) [30, 52–54]. The lattice specific heat,  $C_p$ , in fairly good metals begins to exceed the electronic contribution at a temperature which is a few percent of the Debye temperature [19], and the same must be true for the borocarbides as well. In the Debye model,  $C_p$  tends to a constant value when  $T$  approaches  $\Theta_D$ . It is essential, therefore, to know the  $\Theta_D$ -values for the compounds considered. In the specific heat measurements the following values of  $\Theta_D$  were obtained: 345 K for  $R = \text{Lu}$  [52],  $\approx 540$  K [53] or  $\approx 490$  K [54] for  $R = \text{Y}$ , and 320 K for  $R = \text{Tm}$  [54]. It is evident that  $\Theta_D$ -value for other borocarbides fall within the outlined temperature range. Since most of the thermal conductivity measurements considered below were made in the range 4.2–300 K, it is important to know how  $C_p$  behaves in this range, especially in the high-temperature range 100–300 K. Judging from the above-indicated  $\Theta_D$ -values, a fairly large rise in  $C_p$  with increasing temperature should take place in the high-temperature range. This was found in  $\text{LuNi}_2\text{B}_2\text{C}$  [55], where  $C_p$  has nearly doubled in the range 150–300 K. Although no other specific-heat studies were done (to our knowledge) in the high-temperature range, the same kind of the  $C_p(T)$  behavior must be expected for the other borocarbides as well.

## 2. Thermal Conductivity

The thermal conductivity studies of  $\text{RNi}_2\text{B}_2\text{C}$  compounds are few in number [56–62]. Some of them [56–58, 60, 62] have been made only at very low temperature. Below we consider results on single-crystal borocarbides with  $R = \text{Y}$ ,  $\text{Lu}$ ,  $\text{Yb}$ ,  $\text{Tm}$ ,  $\text{Er}$ ,  $\text{Ho}$ ,  $\text{Dy}$ ,  $\text{Tb}$ , and  $\text{Gd}$ . Certain of the results have been partially presented in Refs. [16, 59, 61]. The samples were provided by P. C. Canfield and his research group at Iowa State University.

### a) Borocarbide magnetic superconductors

Let us start with the magnetic superconductors (R= Dy, Ho, Er, Tm). The temperature behavior of their thermal conductivity is presented in Figs. 3–10. Half of the figures present expanded views of  $\kappa(T)$  and  $\rho(T)$  (and even the absolute thermopower,  $S(T)$ , in Fig. 4) dependences at low temperature. This allows one to follow closely the changes in these properties at phase transitions. On the panels with  $\rho(T)$  curves, the values of  $\rho_{\text{RT}}/\rho_0$  are indicated for characterization of the sample quality.<sup>3</sup> On all figures,  $\kappa_{\text{total}}$  stands for the measured thermal conductivity,  $\kappa_e$  is the WF estimate for the electronic contribution (based on the measured  $\rho$  for these samples), and the remainder,  $\kappa_{\text{total}} - \kappa_e$ , can be thought as being the phonon contribution.

The **DyNi<sub>2</sub>B<sub>2</sub>C** compound transforms from the paramagnetic (PM) into AFM state at the Néel temperature ( $T_N \approx 10.3$  K), which is considerably higher than  $T_C \approx 6.2$  K (see Table I and Refs. [38, 63]), so that this compound goes to the superconducting state already being in the AFM state. The PM-AFM transition is of first order and characterized by very distinct and intensive peak in the temperature dependence of the specific heat [63]. It can be seen from Fig. 4 that the transition results in a reduction by nearly half in the resistivity, and in an appreciable increase in the thermal conductivity and thermopower (in the latter case, the increase is just enormous). The main reason for these dramatic changes is a decrease in the rate of electron scattering by the spin disorder in response to the PM-AFM transition, thus producing the pronounced structure in  $\kappa(T)$ ,  $\rho(T)$  and  $S(T)$  shown in Fig. 4. It is known that spin disorder can give a considerable contribution to the resistivity above  $T_N$  (see the discussion in Ref. [31]). Actually, a relevant spin-disorder term,  $\rho_{\text{sd}}$  (with the electron relaxation rate,  $\tau_{\text{sd}}^{-1}$ ) must be added into Matthiessen's relation (18) for  $T > T_N$ . This term can be reasonable above  $T_N$ , but, for ideal spin alignment below  $T_N$ , it may be thought to be equal to zero. The same reasoning is applicable to the thermal conductivity with the resulting addition of the term  $\tau_{\text{sd}}^{-1}$  to the relation (17). The relaxation rate,  $\tau_{\text{sd}}^{-1}$ , is generally considered to be temperature independent above  $T_N$  [64].

It is evident from Fig. 4 that the main change in the  $\kappa_{\text{total}}(T)$  at the PM-AFM transition can be attributed to that of the electronic contribution,  $\kappa_e$ . Nevertheless, a small dip can be distinguished in the temperature curve of the phonon contribution,

---

<sup>3</sup>  $\rho_0$  here is the value at the temperature  $T_C^+$  at the onset of the resistive superconducting transition, not necessarily the residual resistivity. For R = Tm, Er, Ho it includes the contribution from spin disorder scattering.

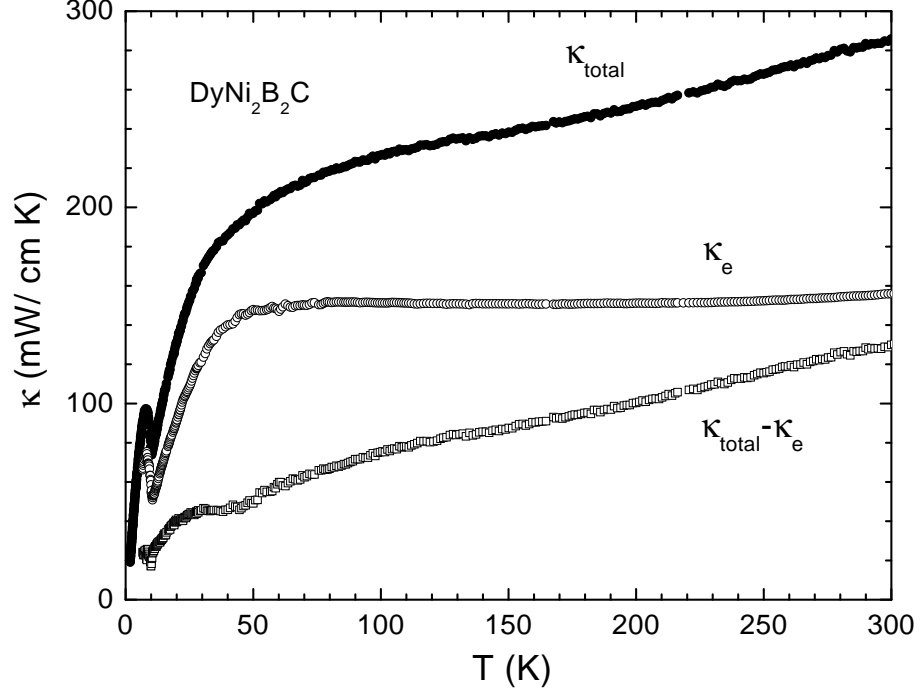


FIG. 3: Temperature dependence of thermal conductivity ( $\kappa_{\text{total}}$ ) for  $\text{DyNi}_2\text{B}_2\text{C}$ . The meaning of  $\kappa_e$  and  $\kappa_{\text{total}} - \kappa_e$  is explained in the main text of the article.

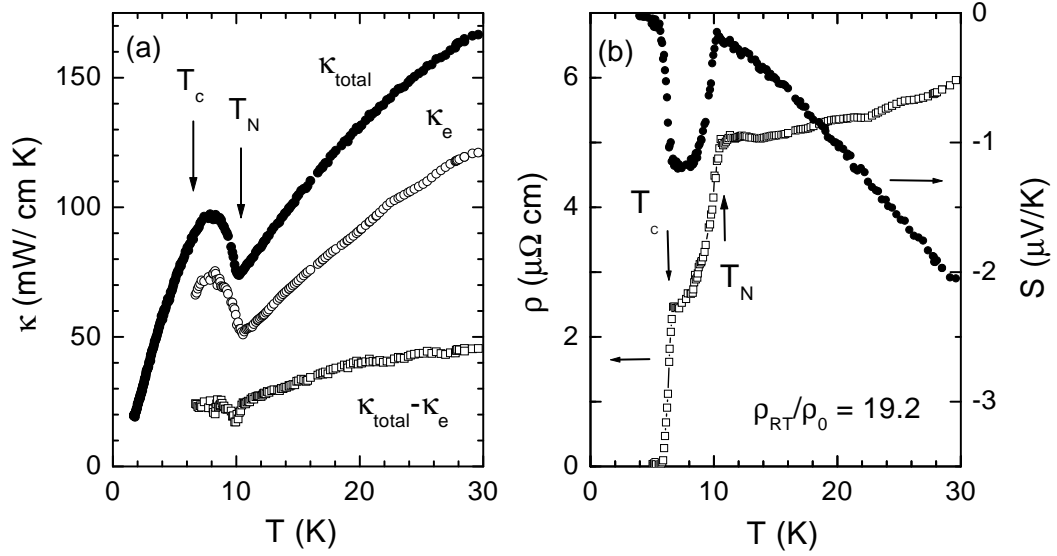


FIG. 4:  $\kappa(T)$  (a),  $\rho(T)$  and  $S(T)$  (b) for  $\text{DyNi}_2\text{B}_2\text{C}$  at low temperature.

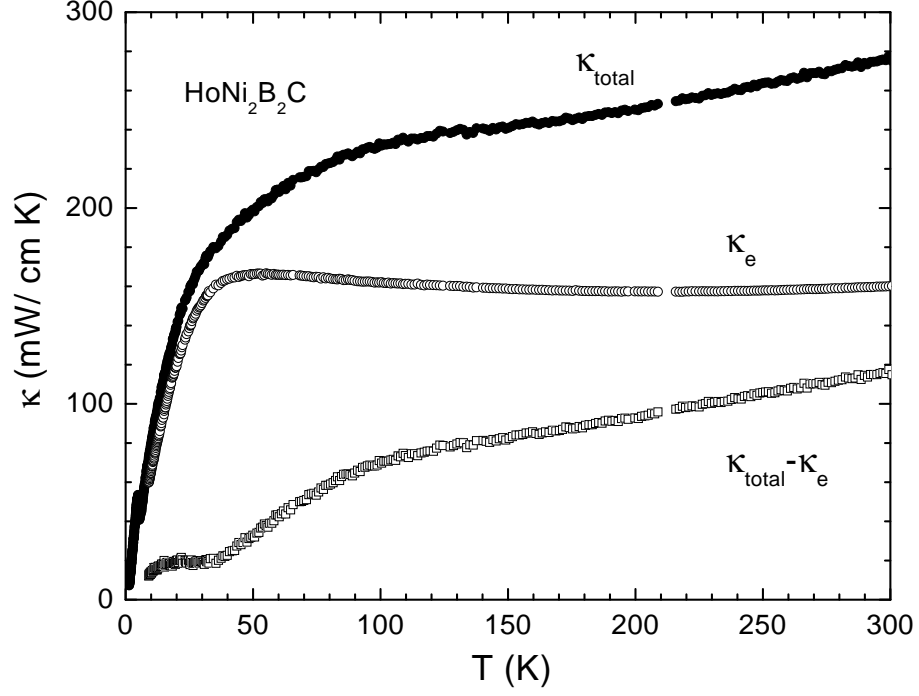


FIG. 5: Temperature dependence of thermal conductivity ( $\kappa_{\text{total}}$ ) for  $\text{HoNi}_2\text{B}_2\text{C}$ . The meaning of  $\kappa_e$  and  $\kappa_{\text{total}} - \kappa_e$  is explained in the main text of the article.

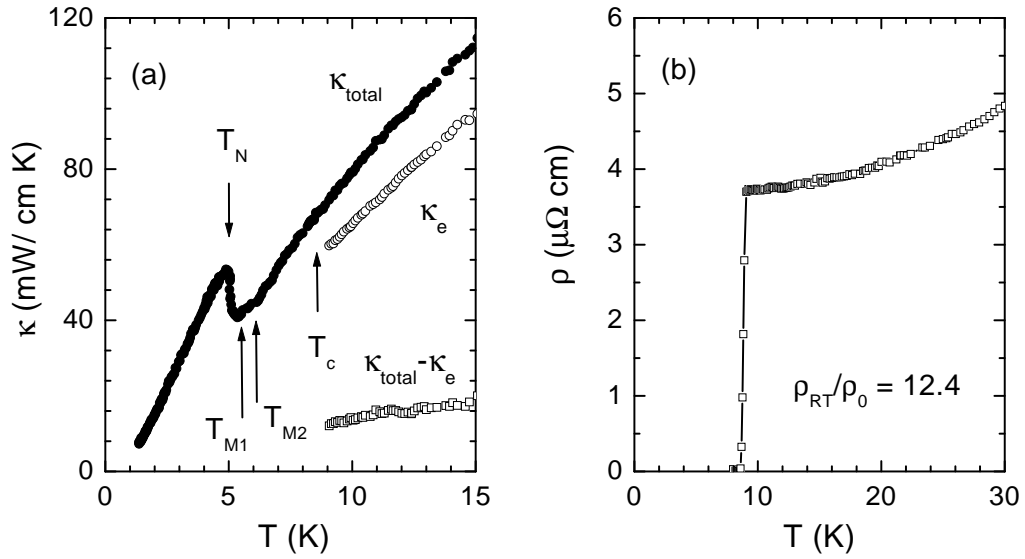


FIG. 6:  $\kappa(T)$  (a) and  $\rho(T)$  (b) for  $\text{HoNi}_2\text{B}_2\text{C}$  at low temperature.

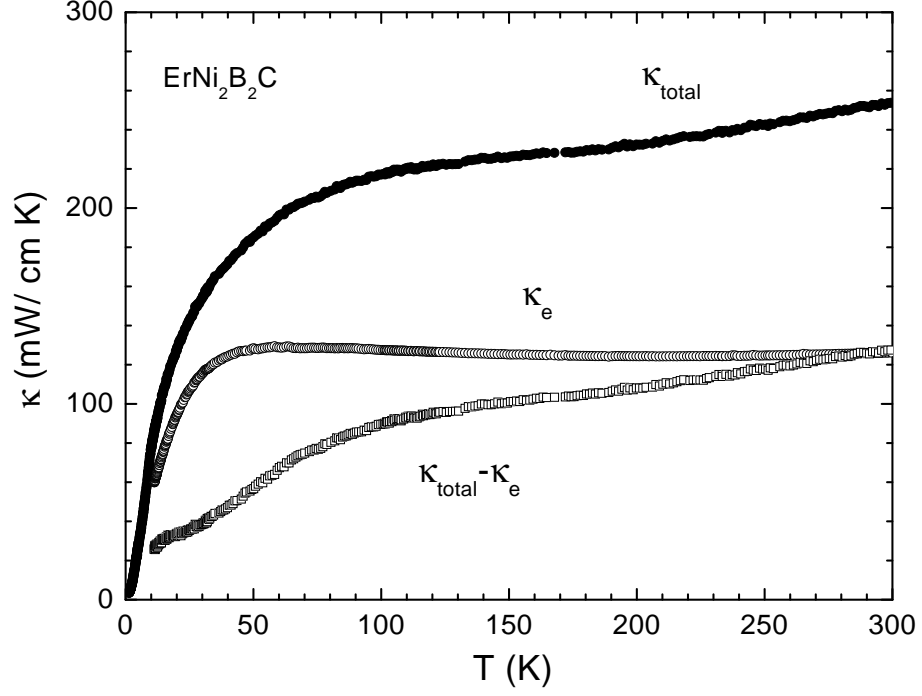


FIG. 7: Temperature dependence of thermal conductivity ( $\kappa_{\text{total}}$ ) for  $\text{ErNi}_2\text{B}_2\text{C}$ . The meaning of  $\kappa_e$  and  $\kappa_{\text{total}} - \kappa_e$  is explained in the main text of the article.

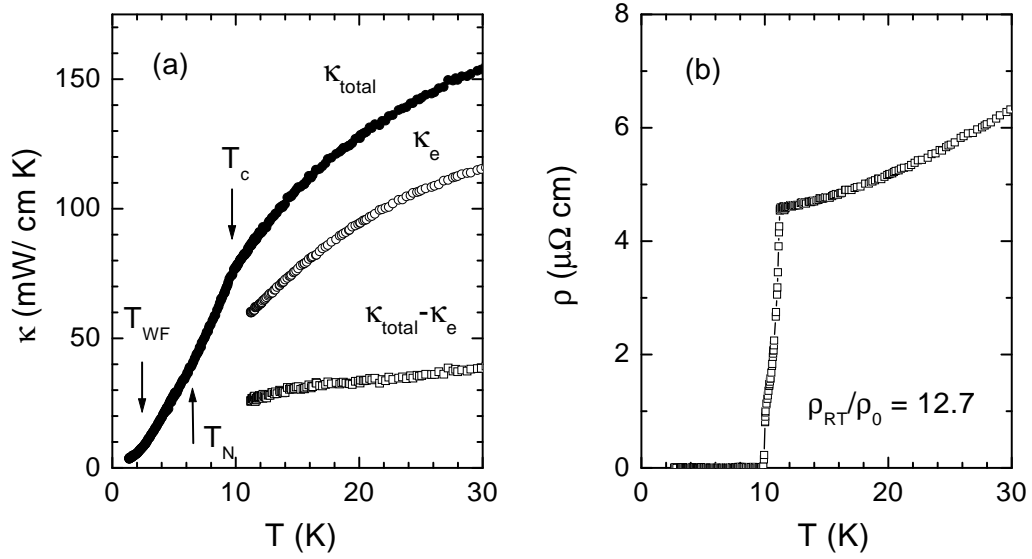


FIG. 8:  $\kappa(T)$  (a) and  $\rho(T)$  (b) for  $\text{ErNi}_2\text{B}_2\text{C}$  at low temperature.

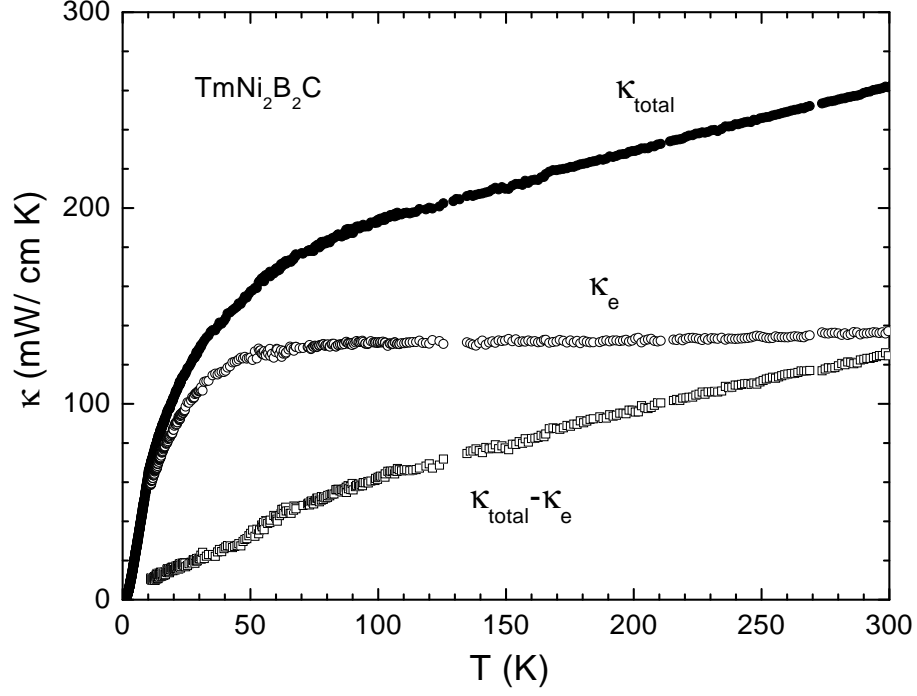


FIG. 9: Temperature dependence of thermal conductivity ( $\kappa_{\text{total}}$ ) for  $\text{TmNi}_2\text{B}_2\text{C}$ . The meaning of  $\kappa_e$  and  $\kappa_{\text{total}} - \kappa_e$  is explained in the main text of the article.

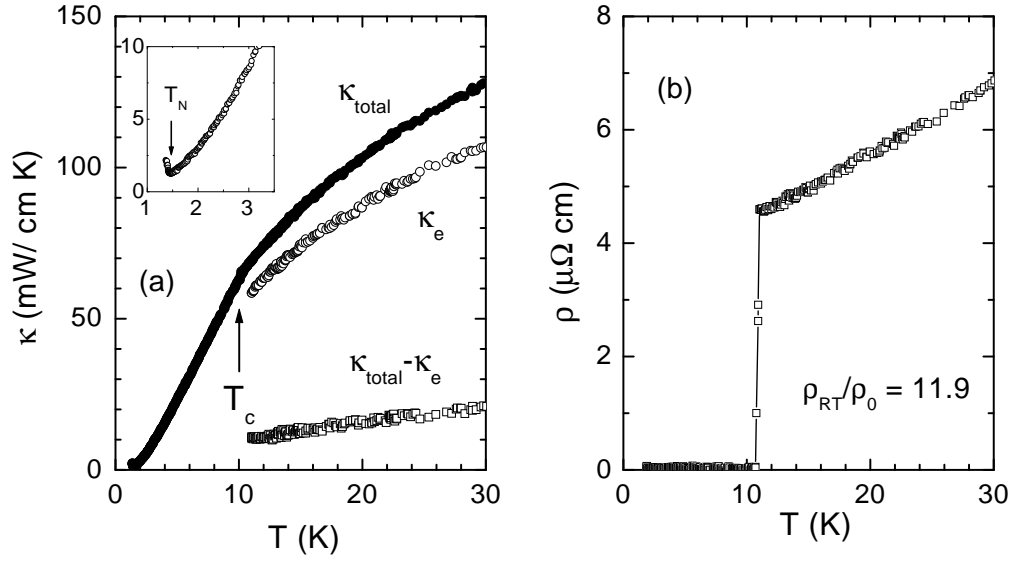


FIG. 10:  $\kappa(T)$  (a) and  $\rho(T)$  (b) for  $\text{TmNi}_2\text{B}_2\text{C}$  at low temperature.

$\kappa_{\text{total}} - \kappa_e$ , in the vicinity of  $T_N$ , as well. The phonon thermal conductivity can be responsive to a magnetic transition when this is accompanied by strong enough magnetoelastic (magnetostriction) effects.

There is no easily discernable change in  $\kappa_{\text{total}}(T)$  at  $T_C$  (Fig. 4). It is possible that rather small changes in slope of  $\kappa(T)$  at  $T_C$  is somewhat hidden on the background of the rapid variation in  $\kappa(T)$  due to the PM-AFM transition. This variation can be appreciable even well below  $T_N$  down to  $T_C$ . This is supported by the point that fairly large changes of  $\rho(T)$  and  $S(T)$  due to this transition occur in the temperature range between  $T_N$  and  $T_C$  [Fig. 4(b)]. No sharp change should be expected either if the electron contribution,  $\kappa_e$ , dominates, and the electrons are scattered predominantly by defects. No abrupt change in slope of  $\kappa_e(T)$  at  $T_C$  occurs in that case [see Fig. 2(a) and discussion in Sec. IIID].

The **HoNi<sub>2</sub>B<sub>2</sub>C** compound has three magnetic transitions below  $T_C \approx 8.5$  K (see Table I and Refs. [38, 65, 66]), so that a coexistence of bulk superconductivity and local long-range magnetic order takes place. The  $\rho(T)$  shows a sharp superconducting transition [Fig. 6(b)], but  $\kappa_{\text{total}}(T)$  does not show a noticeable change in behavior at  $T_C$  [Fig. 6(a)] (the same is found in Ref. [56]). This may be related to defects as the dominant electron scattering mechanism as discussed for the case of DyNi<sub>2</sub>B<sub>2</sub>C (see above), but it is also may be connected with an anomalous superconducting state in the temperature range between  $T_C \approx 8.5$  K and 6.5 K, which was indicated by point-contact tunneling measurements [67]. Of these magnetic transitions, only the transition to the simple AFM state at  $T_N \approx 5.2$  K produces an appreciable feature in the  $\kappa_{\text{total}}(T)$  curve [Fig. 6(a)]. The other two [their transition temperatures are denoted by  $T_{M1}$  and  $T_{M2}$  in Fig. 6(a)] have a minimal effect on the thermal conductivity. A change in slope at  $T_{M2}$  is clearly visible, but any feature at  $T_{M1}$  is within the noise. It is interesting that the specific heat ( $C$ ) behaves somewhat in a similar manner at these transitions [65, 66]. Whereas, a sharp and intensive peak in  $C(T)$  is found at  $T = T_N$  [65, 66], there are only weak discernible shoulders in the  $C(T)$  dependences at the temperatures  $T_{M1}$  and  $T_{M2}$  [30, 65]. The reason is that AFM transition at  $T_N$  is of first order [66]; whereas, the other two are of second one. It is clear that first-order magnetic transitions, characterized by discontinuous changes in the magnetic entropy (see Refs. [63, 65] for borocarbides) and in the compound density, should lead to more significant change in the thermal conductivity of the borocarbides than the second-order ones (characterized by discontinuous changes in the second derivatives of the Gibbs free energy, such as the volume thermal expansivity or the specific heat).

The **ErNi<sub>2</sub>B<sub>2</sub>C** borocarbide transforms with decreasing temperature first into the superconducting state at  $T_C \approx 11$  K, then into a MAFM state at  $T_N \approx 6.8$  K (first order transition), and finally into a WFM state at  $T_{WF} \approx 2.3$  K (second order transition) (see

Table I and Refs. [38, 40, 68]). For this compound a rather distinct change in the slope of  $\kappa_{\text{total}}(T)$  at  $T_C$  can be seen [Fig. 8(a)], consistent with measurements on polycrystalline  $\text{ErNi}_2\text{B}_2\text{C}$  sample by Cao *et al.* [57]. But no features can be distinguished in the  $\kappa_{\text{total}}(T)$  curve at  $T_N$  and  $T_{\text{WF}}$ .

The **TmNi<sub>2</sub>B<sub>2</sub>C** compound is superconducting below  $T_C \approx 11$  K, and undergoes a MAFM transition (of first order) below  $T_N \approx 1.5$  K (see Table I and Refs. [38, 54, 69]). A rather clear kink is seen in the  $\kappa_{\text{total}}(T)$  curve at  $T_C$ , which corresponds in Fig. 10(a) to the temperature of the superconducting transition from the  $\rho(T)$  data. A sharp increase in the thermal conductivity is readily seen at about 1.4 K, that is slightly below  $T_N$  [see insert in Fig. 10(a)]. It is particularly remarkable that  $\kappa_{\text{total}}$  doubles in a very short temperature range. It is clear that this increase is determined by the transition to the AFM state.  $T_N$  is, however, much less than  $T_C$  ( $T_N/T_C \approx 0.136$ ) and, therefore, the fraction of the normal electrons (which remain heat carriers below  $T_C$ , see Sec. IIID) must be very small below  $T_N$ . For this reason, the explanation given above in the case of  $\text{DyNi}_2\text{B}_2\text{C}$  (an abrupt decrease in the rate of electron scattering by the spin disorder below  $T_N$ ), is inapplicable for  $\text{TmNi}_2\text{B}_2\text{C}$ . Really, the theoretical calculations [see Refs. [22, 24] and Fig. 2(a)] show that  $\kappa_e$  is negligibly small for  $T_N/T_C < 0.2$ .

The transition of  $\text{TmNi}_2\text{B}_2\text{C}$  into the AFM state does not destroy its global superconductivity in the sense that the resistivity remains zero [54]. But it could suppress the superconducting state in such way (causing the effective  $T_C$  to become less than 11 K) that the fraction of the normal electrons would increase rather abruptly below  $T_N$ . Together with disappearing of the spin-disorder electron scattering below  $T_N$ , this could lead to an appreciable increase in  $\kappa_e$ . A considerable decrease in the upper critical field  $H_{c2}$  (parallel to the  $ab$  plane) found in  $\text{TmNi}_2\text{B}_2\text{C}$  below 3 K [31, 70] gives some support to this suggestion. According to Ref. [69], the Tm moments order below 1.5 K with an incommensurate magnetic structure consisting of Tm moments, aligned ferromagnetically along the  $c$  axis in the (110) planes, and the magnitude of the moments modulated sinusoidally along the diagonal of the  $ab$  plane. This magnetic structure should, however, support magnons. The formation of the magnons, which are heat carriers and whose number is especially large in the temperature range just slightly below  $T_N$ , also could explain the sharp rise in  $\kappa_{\text{total}}$  below  $T_N$ . It is hard to judge at the moment, however, the possible relative contributions, if any, of these two inferred mechanisms without some additional experimental studies.

Let us survey now the general features of the thermal conductivity behavior in the borocarbide magnetic superconductors ( $R = \text{Dy}, \text{Ho}, \text{Er}, \text{Tm}$ ) in the temperature range above both,  $T_C$  and  $T_M$  (Figs. 3, 5, 7, and 9). It can be said that the electron contribution to

the thermal conductivity,  $\kappa_e$ , clearly dominates over the phonon one,  $\kappa_{\text{total}} - \kappa_e$ , only at low temperature ( $< 50$  K), but with increasing temperature the relative phonon contribution grows significantly, so that at room temperature these contributions are quite comparable (if not nearly equal). The  $\kappa_e(T)$  is approximately constant for  $T > 100$  K, as expected according to Eq. (13) for electronic thermal conductivity and the WF law (16) in the case of linear  $\rho(T)$  dependence (which is approximately obeyed in this temperature range for all of the borocarbides mentioned). But there is no peak in the  $\kappa_e(T)$  dependence which is expected below  $0.1 \Theta_D$  for good enough metals (see Sec. III B). The reason is that the borocarbides are maybe not good enough metals to the extent that they should show this peak. Really, the highest thermal conductivity magnitude of borocarbides is generally below  $0.3$  W/cmK (see Figs. 3, 5, 7, 9 above and figures for other samples below). At the same time, the silver foil presented in Fig. 1 has a peak of about  $14$  W/cmK at  $T_{\text{max}} \approx 16$  K in the  $\kappa(T)$  curve. The silver samples with a highest degree of perfection have a peak value as high as  $200$  W/cmK with  $T_{\text{max}} \approx 7$  K, but no peak at all can be found in the  $\kappa(T)$  dependences of the fairly imperfect silver samples with thermal conductivity below  $2$ – $3$  W/cmK [15]. An identical picture of the lattice-disorder influence was found for copper samples [28]. The thermal conductivity of the borocarbides is expected to be far (at least, one order of magnitude) less than that of the noble metals, since these latter have higher electron density and their electrons have a far greater Fermi velocity. The thermal conductivity of the transition metals is also far (one or even two order of magnitude) less than that of the noble metals. For these metals the peak in  $\kappa(T)$  curves is not so sharp and is usually found only in the most perfect samples with  $\kappa$  above  $0.4$ – $1.0$  W/cmK [15]). In some transition metals with very low thermal conductivity (Mn and V) the peak was not found at all [15]. It can be suggested, therefore, that the absence of a peak for the borocarbide  $\kappa(T)$  curves is determined mainly by lattice defects.

Consider now the temperature behavior of the phonon part,  $\kappa_{\text{total}} - \kappa_e = \kappa_p$ , of the thermal conductivity, presented in Figs. 3, 5, 7, and 9 by the  $\kappa_{\text{total}} - \kappa_e$  curves. According to the general relation (7), the  $\kappa_p$  is determined by phonon-phonon (PP), phonon-imperfection (PI) and phonon-electron (PE) interactions. The PP interaction should result in formation of a peak in the  $\kappa_p(T)$  dependence at  $T_{\text{max}} < 0.1 \Theta_D$ , which, however, can be depressed or totally smeared by strong enough lattice disorder. The shoulders, clearly seen in Figs. 3, 5, and 9 for  $R = \text{Dy}$ ,  $\text{Ho}$ , and  $\text{Tm}$  in the range  $35$ – $45$  K, could be indicators of the peak in the case of rather strong lattice disorder. As temperature increases above  $T_{\text{max}}$ , the PP interaction can only induce a decrease in  $\kappa_p(T)$  (see Sec. III A). This is inconsistent with the temperature behavior of the  $\kappa_{\text{total}} - \kappa_e$  curves (Figs. 3, 5, 7, and 9), which suggests that  $\kappa_p$  rises steadily with temperature increasing up to room temperature.

This rise can be determined by other (PI and PE) mechanisms of phonon scattering. If the PI interaction is taken into account, the point defects can be assumed as the most important imperfections in the single-crystal borocarbides [51]. In the intermediate temperature range below  $\Theta_D$ , the phonon wavelength decreases with increasing temperature approaching an interatomic distance. In this case the temperature dependence of the PI relaxation rate is expected to be rather weak. On the other hand, the specific heat,  $C_p$ , of borocarbides rises significantly in this range (see discussion in Sec. IV A 1). This can determine (or, at least, contribute to) the rise in  $\kappa_p$  with increasing temperature. Another source of this increase in  $\kappa_p$  can be found in the PE interaction (see Sec. III C). According to Eq. (23), the corresponding term,  $\kappa_{pe}$ , grows with increasing temperature for all temperatures below  $\Theta_D$ , and this growth can be profound in the intermediate temperature range. It is important as well that in this range the term  $\kappa_{pe}$  can be comparable with the electronic thermal conduction (see discussion in Sec. III C). In this way the both, the PI interaction and the PE one, can contribute to the growth of the thermal conductivity of the borocarbides with increasing temperature.

#### b) Purely superconducting borocarbides

Up to this point the properties of magnetic superconductors ( $R = \text{Dy, Ho, Er, Tm}$ ) has been considered. It is interesting to compare their behavior with that of the superconducting borocarbides without magnetic order, **YNi<sub>2</sub>B<sub>2</sub>C** and **LuNi<sub>2</sub>B<sub>2</sub>C**, with  $T_C$ 's 15.6 and 16.6 K, respectively. Both of them are believed to be clean-limit type II superconductors [32, 33, 71]. Neither Y nor Lu are magnetic and neither YNi<sub>2</sub>B<sub>2</sub>C nor LuNi<sub>2</sub>B<sub>2</sub>C exhibit any magnetic order [38]. No AFM correlations or local magnetic moments of nickel are present in YNi<sub>2</sub>B<sub>2</sub>C [72]. Inelastic neutron scattering measurements show soft phonon modes below  $T_C$  for YNi<sub>2</sub>B<sub>2</sub>C [73] and LuNi<sub>2</sub>B<sub>2</sub>C [74]. A model phonon spectra was presented in Ref. [30] based on specific heat measurements [55]. A very pronounced low temperature softening of the low energy optical phonons and the transverse acoustic modes was found. The thermal conductivity of these compounds was studied at low temperature in Refs. [56] (YNi<sub>2</sub>B<sub>2</sub>C) and [58, 60] (LuNi<sub>2</sub>B<sub>2</sub>C).

The general behavior of  $\kappa(T)$  for LuNi<sub>2</sub>B<sub>2</sub>C is shown in Fig. 11. Nearly the same picture is found for YNi<sub>2</sub>B<sub>2</sub>C (and not shown in this paper for this reason). The low temperature behavior of  $\kappa(T)$  and  $\rho(T)$  is presented in Fig. 12 for both compounds. Figure 11 indicates that at temperature below  $T \simeq 60$  K the WF estimate for the electronic

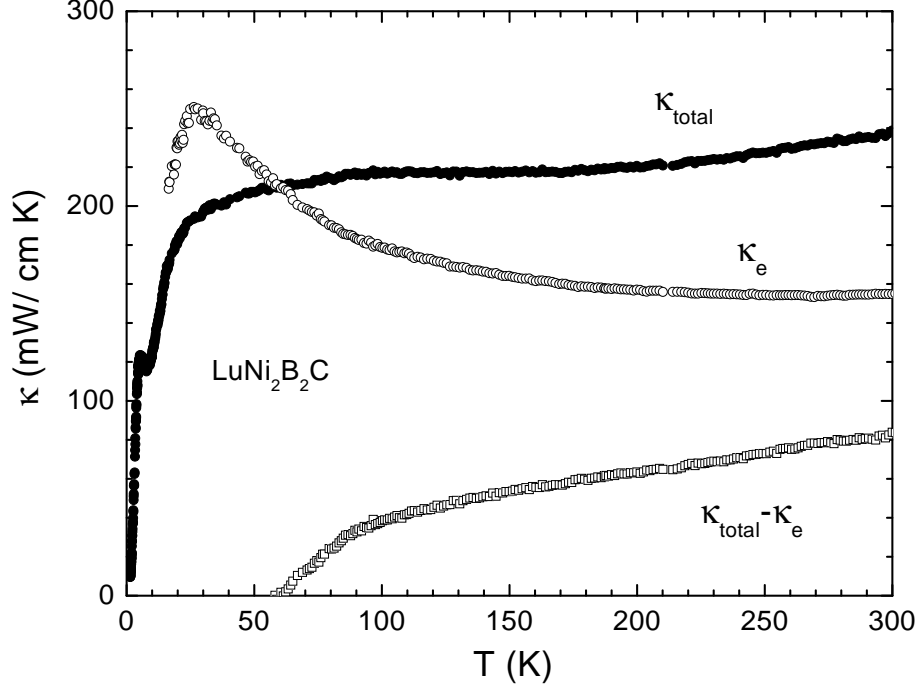


FIG. 11: Temperature dependence of thermal conductivity ( $\kappa_{\text{total}}$ ) for  $\text{LuNi}_2\text{B}_2\text{C}$ . The meaning of  $\kappa_e$  and  $\kappa_{\text{total}} - \kappa_e$  is explained in the main text of the article.

contribution,  $\kappa_e$ , is greater than the total measured thermal conductivity.<sup>4</sup> Obviously this is caused by the breakdown of the WF law in the intermediate temperature range due to inelastic electron-phonon scattering (see Sec. III B). Really, the effective Lorenz number,  $L$ , in this temperature range could be much less than  $L_0$ , used for calculation of the  $\kappa_e$  (see Eq.(16) and Refs. [14, 17]). The study of  $\kappa(T)$  of a single-crystal  $\text{LuNi}_2\text{B}_2\text{C}$  by Boaknin *et al.* [58] also implies reduced values of  $L$  below 100 K. The deviations from the WF law are less for metals with increased lattice (or spin) disorder (see Sec. III B). Perhaps for this reason the breakdown of the WF law does not manifest itself so clearly in the magnetic borocarbides, which have higher resistivity in this temperature range than these of  $\text{YNi}_2\text{B}_2\text{C}$  and  $\text{LuNi}_2\text{B}_2\text{C}$ . It is interesting, however, that the  $\kappa_e(T)$  behavior of  $\text{LuNi}_2\text{B}_2\text{C}$  (Fig. 11) corresponds to one typical of electronic thermal conductivity for fairly good metals, and, among other things, shows a maximum at  $T_{\text{max}} \simeq 25$  K which is expected at  $T \leq 0.1\Theta_D$  (see Sec. III B). ( $\Theta_D$  is about 345 K for  $\text{LuNi}_2\text{B}_2\text{C}$  [52]). This maximum (which was found for  $\text{YNi}_2\text{B}_2\text{C}$  as well) gives further evidence that these samples are well ordered.

The superconducting transitions for  $\text{LuNi}_2\text{B}_2\text{C}$  and  $\text{YNi}_2\text{B}_2\text{C}$  are rather clearly indi-

<sup>4</sup> The same behavior is found for  $\text{YNi}_2\text{B}_2\text{C}$  for  $T \leq 80$  K.

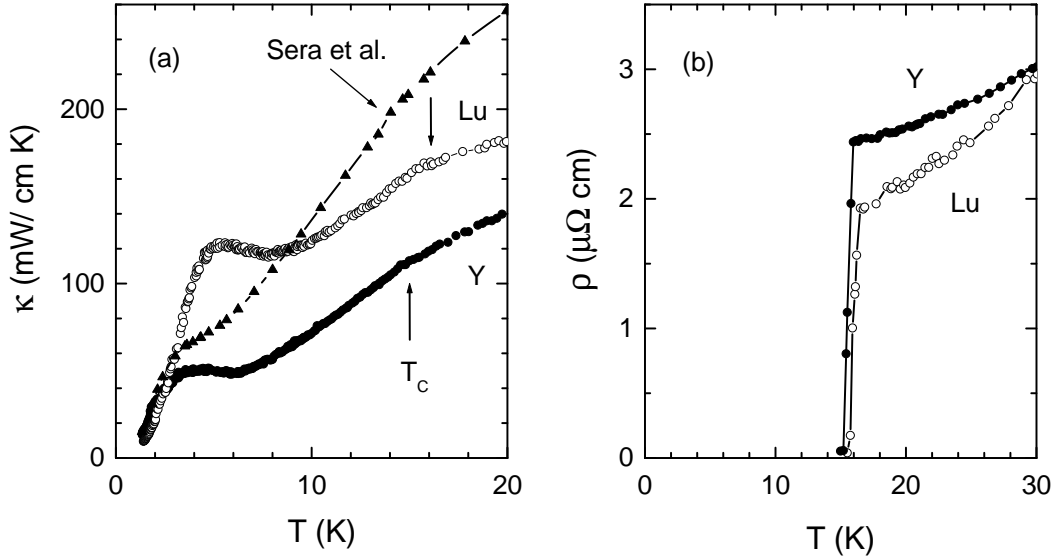


FIG. 12:  $\kappa(T)$  (a) and  $\rho(T)$  (b) dependences for LuNi<sub>2</sub>B<sub>2</sub>C ( $\rho_{RT}/\rho_0 = 24.9$ ) and YNi<sub>2</sub>B<sub>2</sub>C ( $\rho_{RT}/\rho_0 = 16.5$ ) at low temperature. The left panel (a) shows also the  $\kappa(T)$  data for YNi<sub>2</sub>B<sub>2</sub>C obtained by Sera *et al.* [56].

cated in  $\kappa(T)$  [Fig. 12(a)]. Both of the compounds show a strong enhancement in  $\kappa$  below  $T_C$ . The evident explanation is an increase in the phonon thermal conductivity due to reduced phonon-electron scattering as the normal electrons condense into Cooper pairs (see Sec. IIID). The same behavior [that is a phonon-induced peak in the  $\kappa(T)$  below  $T_C$ ] was observed by Boaknin *et al.* for LuNi<sub>2</sub>B<sub>2</sub>C [58]; whereas Sera *et al.* [56] have found only a “shoulder” in  $\kappa(T)$  below  $T_C$  for YNi<sub>2</sub>B<sub>2</sub>C which can be easily suppressed by an external magnetic field [Sera *et al.* data for zero field are shown in Fig. 12(a)]. It is obvious that the peak magnitude and its position depends on the relative importance of other scattering mechanisms. In fact, the  $\kappa(T)$  curves in Fig. 12(a) correspond to the case considered in Sec. IIID when both kinds of the heat carriers (electrons and phonons) compete on equal terms [see Fig. 2(b)]. Taking into account Eqs. (13) and (14), the ratio of electronic thermal conductivities in superconducting and normal states,  $\kappa_e^s/\kappa_e^n$ , below  $T_C$  can be presented as

$$\kappa_e^s/\kappa_e^n = n_n(T)/n_e,$$

where  $n_e$  is the electron density,  $n_n(T)$  is the density of normal electrons below  $T_C$  which decreases as temperature goes down away from  $T_C$ . In the same way [assuming domination of the phonon-electron scattering and using Eq. (23)] the following relation can be written for the ratio of phonon thermal conductivities in the superconducting and normal states

below  $T_C$ :

$$\kappa_p^s/\kappa_p^n = n_e/n_n(T).$$

It is seen that a decrease in  $n_n$  below  $T_C$  leads to continuous reduction in the ratio  $\kappa_e^s/\kappa_e^n$  for the electronic contribution; whereas, the ratio  $\kappa_p^s/\kappa_p^n$  for the phonon contribution rises, causing an increase in the phonon thermal conductivity (see Sec. IIID). The competition of these two mechanisms can result in the  $\kappa(T)$  behavior shown in Fig. 12(a).

Measurement of the thermal conductivity at very low temperatures in an applied magnetic field ( $H_{c1} \leq H \leq H_{c2}$ ) provides a very powerful tool for study of the symmetry of the superconducting gap function. At very low temperature it is somewhat easier to sort out the contributions to  $\kappa(T)$  from the charge carriers and the phonons. In an ordinary BCS type II superconductor the normal charge carriers are localized in the vortex cores and can only tunnel between them in the mixed state. Thus the electronic thermal conductivity is expected to increase very slowly at low field. But as the field approaches  $H_{c2}$ , the vortices are much closer. The tunneling, then, becomes more pronounced and the electronic contribution increases rapidly with applied field (see general description of the magnetic-field effects in the thermal conductivity below  $T_C$  in Ref. [1]). If, however, there are nodes in the gap function,  $\kappa(T, H)$  increases rapidly for even small fields above  $H_{c1}$ , since there will be delocalized normal electrons to couple the vortex cores, even at very low temperature. Recent thermal conductivity measurements at low temperature for single crystal  $\text{LuNi}_2\text{B}_2\text{C}$  [60] and  $\text{YNi}_2\text{B}_2\text{C}$  [62] samples exhibit dramatically enhanced thermal conductivity at rather small applied fields. Both experiments suggest a highly anisotropic gap function for these borocarbides. For  $\text{LuNi}_2\text{B}_2\text{C}$  the data appear to suggest the possibility of a line of nodes in the gap; whereas, the experiment with  $\text{YNi}_2\text{B}_2\text{C}$  has been interpreted in terms of point nodes along the  $a$  and  $b$  axes. These experiments certainly challenge the view that these materials are  $s$ -wave BCS superconductors.

### c) Purely magnetic borocarbides

Borocarbides  $\text{TbNi}_2\text{B}_2\text{C}$  and  $\text{GdNi}_2\text{B}_2\text{C}$  are magnetic at low enough temperature (see Table I), but not superconducting (at least above 0.3 K). The absence of superconductivity is supposed to be caused by  $4f$  magnetic moments [33]. The temperature behavior of thermal conductivity for these compounds is presented in Figs. 13 and 15. Expanded views of  $\kappa(T)$ ,  $\rho(T)$  and  $S(T)$  dependences at low temperature are shown in Figs. 14 and 16.

Two magnetic transitions have been found for  $\text{TbNi}_2\text{B}_2\text{C}$ : (1) transition (of first order)

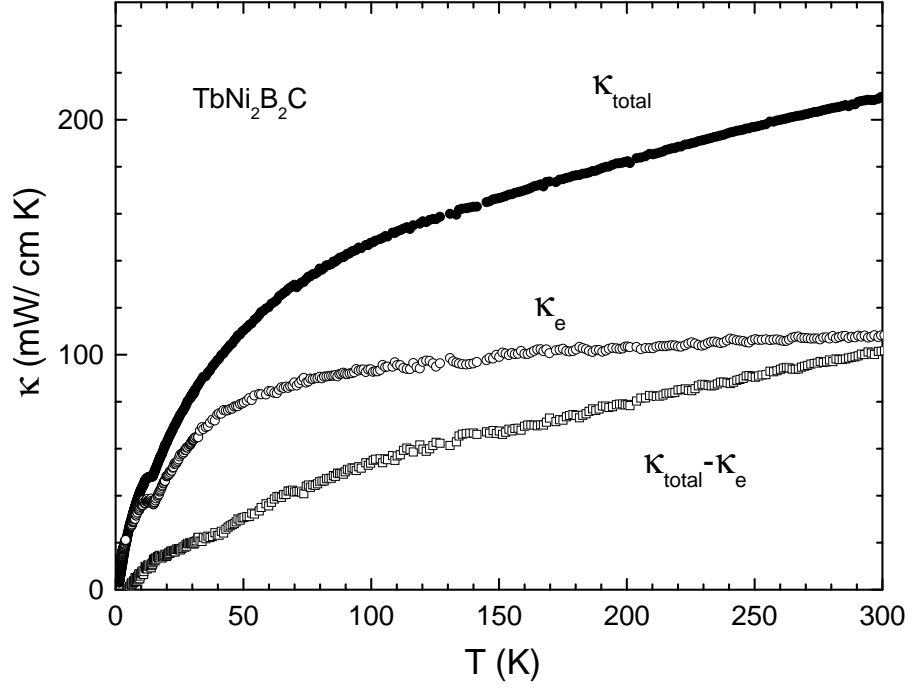


FIG. 13: Temperature dependence of thermal conductivity ( $\kappa_{\text{total}}$ ) for  $\text{TbNi}_2\text{B}_2\text{C}$ . The meaning of  $\kappa_e$  and  $\kappa_{\text{total}} - \kappa_e$  is explained in the main text of the article.

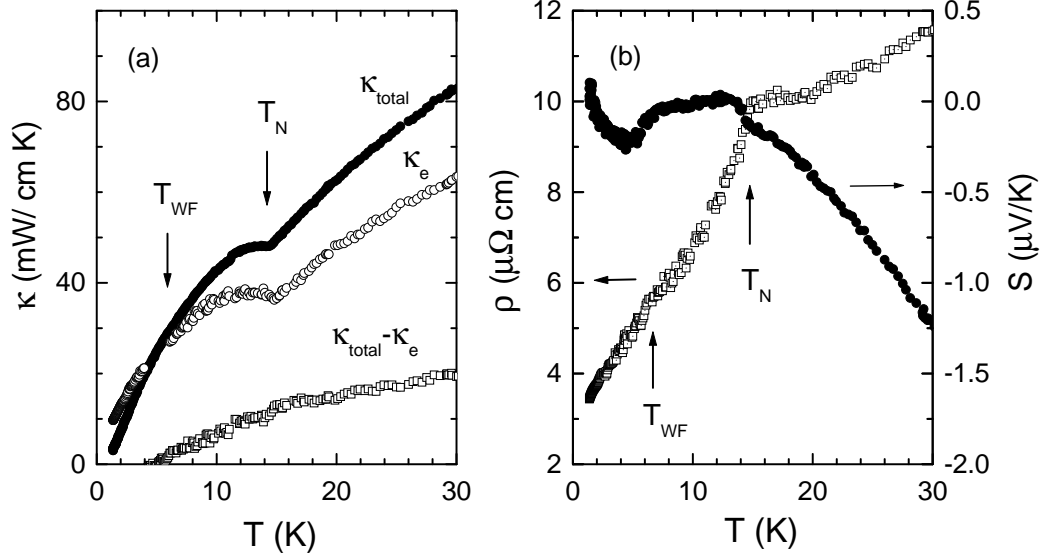


FIG. 14:  $\kappa(T)$  (a),  $\rho(T)$  and  $S(T)$  (b) for  $\text{TbNi}_2\text{B}_2\text{C}$  at low temperature. The magnetic residual resistivity ratio,  $\rho(300\text{K})/\rho(T_N)$  is 6.8. Using  $\rho$  at the lowest temperature measured,  $\rho_{\text{RT}}/\rho_0 = 19.7$  can be obtained.

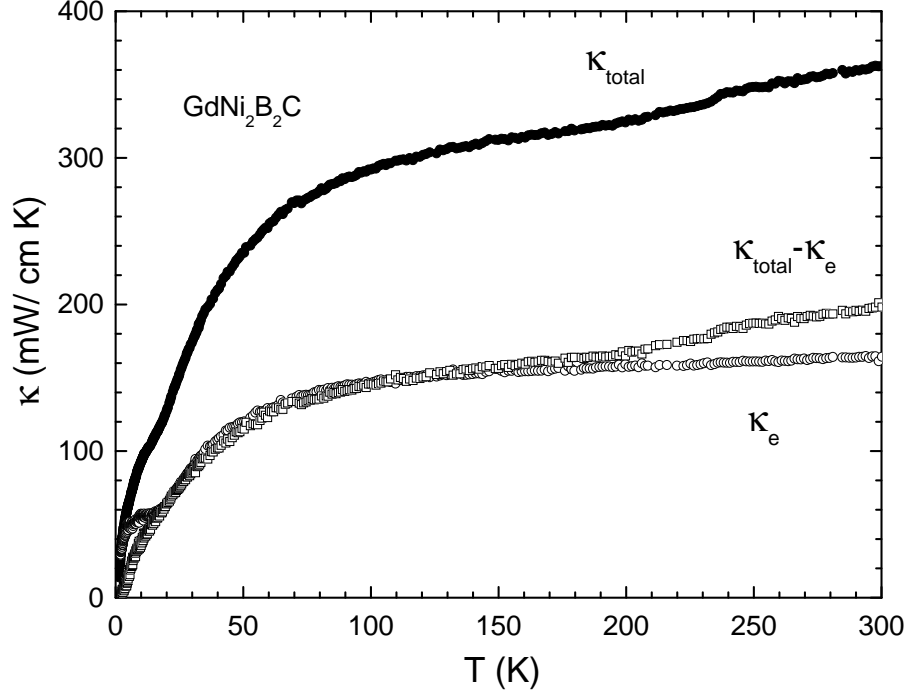


FIG. 15: Temperature dependence of thermal conductivity ( $\kappa_{\text{total}}$ ) for  $\text{GdNi}_2\text{B}_2\text{C}$ . The meaning of  $\kappa_e$  and  $\kappa_{\text{total}} - \kappa_e$  is explained in the main text of the article.

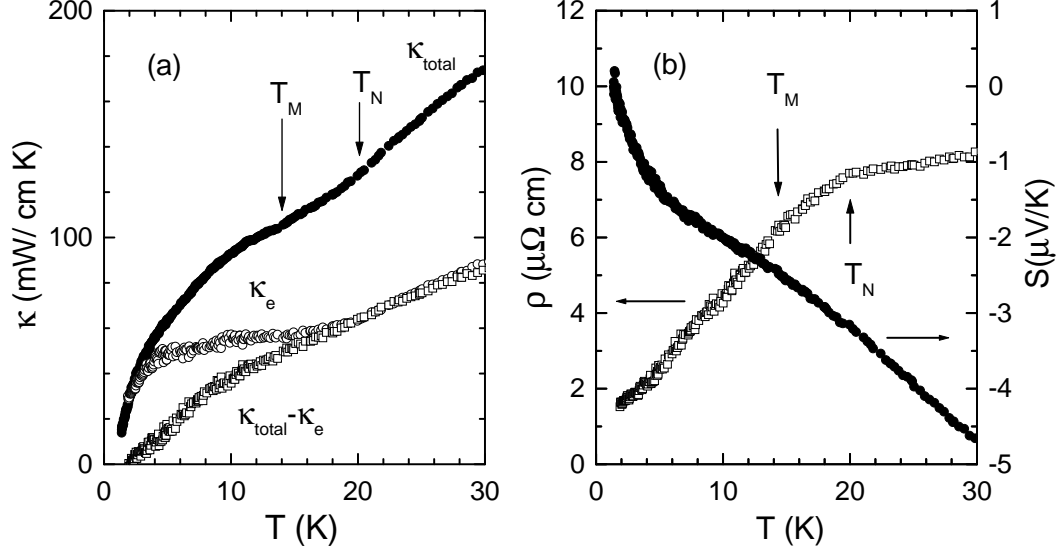


FIG. 16:  $\kappa(T)$  (a),  $\rho(T)$  and  $S(T)$  (b) dependences for  $\text{GdNi}_2\text{B}_2\text{C}$  at low temperature. The magnetic residual resistivity ratio,  $\rho(300\text{K})/\rho(T_N)$  is 5.8. Using  $\rho$  at the lowest temperature measured,  $\rho_{\text{RT}}/\rho_0 = 29.7$  can be obtained.

from paramagnetic to modulated AFM state below  $T_N \approx 15$  K with the magnetic moments lying along the  $a$  direction, and (2) transition (of second order) to WFM state below  $T_{WF} = 6-8$  K with the magnetic moments lying along the  $\langle 100 \rangle$  or  $\langle 110 \rangle$  directions in the  $ab$  plane under applied magnetic fields [38, 41, 75]. The transition to the modulated AFM state is clearly indicated in the  $\kappa(T)$ , and causes strong changes in  $\rho(T)$  and  $S(T)$  curves (Fig. 14). This can be explained in the same way as for  $\text{DyNi}_2\text{B}_2\text{C}$  and  $\text{HoNi}_2\text{B}_2\text{C}$  by an appreciable decrease in the rate of electron scattering by the spin disorder in response to PM-AFM transition (see discussion above). Since in this compound the electronic contribution to the thermal conductivity,  $\kappa_e$ , clearly dominates over the phonon one,  $\kappa_{\text{total}} - \kappa_e$ , for the low temperature range (see Fig. 13), the measured thermal conductivity,  $\kappa_{\text{total}}$ , can exhibit a clear response to this change in the electron scattering rate. The second-order AFM-WFM transition at  $T_{WF}$  is not indicated in  $\kappa(T)$  dependence, although weak change in  $\rho(T)$  and rather appreciable change in  $S(T)$  (both around  $T \approx 7$  K) are clearly seen (Fig. 14). The absence of some feature in  $\kappa(T)$  at  $T_{WF}$  can be explained by the fact that this transition does not strongly effect the scattering of charge carriers and has no influence on the phonon scattering.

The borocarbide  $\text{GdNi}_2\text{B}_2\text{C}$  transforms into modulated AFM state below  $T_N \approx 20$  K (first-order transition), with the magnetic moments lying in the  $b$  direction [76, 77]. With further decreasing temperature it goes into another modulated AFM state below  $T_M \approx 13.6$  K (second-order transition), with the magnetic moments tilting somewhat into the  $c$  direction [76, 77]. The measured  $\kappa_{\text{total}}(T)$  dependence shows a subtle change in its slope at  $T_N$  (Fig. 16), which is less clear than that for  $\text{TbNi}_2\text{B}_2\text{C}$  (Fig. 14). The weak feature in  $\kappa(T)$  at  $T_N$  for  $\text{GdNi}_2\text{B}_2\text{C}$  was found also for polycrystalline samples in Ref. [57]. This weak sensitivity of  $\kappa(T)$  to first-order AFM transition can be partly explained by the fact that the electronic contribution to total  $\kappa$  for this compound is much less than that of in  $\text{TbNi}_2\text{B}_2\text{C}$  (compare Figs. 13 and 15) and (especially) in  $\text{DyNi}_2\text{B}_2\text{C}$  and  $\text{HoNi}_2\text{B}_2\text{C}$  (see Figs. 3 and 5), where the magnetic transitions of this type produce quite appreciable changes in  $\kappa(T)$  at  $T_N$  (Figs. 4 and 6). The transition to another MAFM state below  $T_M \approx 14$  K produces only subtle changes in  $\kappa(T)$ ,  $\rho(T)$  and  $S(T)$  of  $\text{GdNi}_2\text{B}_2\text{C}$  (Fig. 16). The explanation of this fact is the same as indicated above for  $\text{TbNi}_2\text{B}_2\text{C}$ , i.e., the transition appears to only slightly affect the scattering of charge carriers and has no influence on the phonon scattering. It is interesting to note that here is no indication of  $T_N$  in the phonon contribution for  $R = \text{Tb}$  or  $\text{Gd}$ , unlike the small dip at  $T_N$  in the phonon contribution for  $R = \text{Dy}$  shown in Fig. 4. This suggests that the nature of the transitions for the former two materials is different in regards to its influence on the phonon contributions. An alternate explanation is that the small dip in Fig. 4 for

DyNi<sub>2</sub>B<sub>2</sub>C is an artifact of using the WF law in the region where  $\rho(T)$  is varying so rapidly with temperature. Any small variations in temperature between the  $\rho(T)$  and  $\kappa(T)$  measurements would create this dip.

#### d) Heavy-fermion borocarbide YbNi<sub>2</sub>B<sub>2</sub>C

YbNi<sub>2</sub>B<sub>2</sub>C is neither superconducting (above 0.05 K [78]) nor orders magnetically (above 0.023 K [39]). The compound is a heavy-fermion system [39, 79, 80] with a Kondo temperature of  $T_K \approx 10$  K and with a Sommerfeld coefficient of  $\gamma \simeq 530$  mJ/(mole K<sup>2</sup>) [79]. When compared to that of LuNi<sub>2</sub>B<sub>2</sub>C ( $\gamma \approx 19$  mJ/(mole K<sup>2</sup>) [52, 55]) this corresponds to an effective mass almost 30 times larger than that for the Lu-based compound provided that  $k_F$  is approximately the same for all members of the series. The magnetic susceptibility is anisotropic and exhibits Curie-Weiss [ $1/(T - \theta_{CW})$ ] behavior at high temperature with a negative value of  $\theta_{CW}$ , indicative that AFM correlations play a significant role. This behavior is consistent with the interpretation of a highly correlated ground state at low temperatures and crystal electric field effect at higher temperatures [78]. Recent neutron scattering experiments of Boothroyd *et al.* [81] indicate that the crystal electric field is significantly enhanced over that of the other family members and produces a temperature dependent effective Kondo interaction. These authors found a Kondo temperature of 25 K compared to the  $T_K = 10$  K, obtained from specific heat and susceptibility measurements [79], and they also suggest that at  $T = 0$  the compound might be close to a quantum critical point on the non-magnetic side. The electrical resistivity exhibits a quadratic temperature dependence below 1.5 K [79], and the ratio of the coefficient of the quadratic term to the  $\gamma^2$  is approximately that found for UPt<sub>3</sub> along its hexagonal axis [79]. These results all suggest that hybridization between the Yb 4*f* and conduction electron states is responsible for the suppression of superconductivity in this borocarbide [79] even though a simple de Gennes scaling argument [79, 80] would suggest that it should be superconducting at about 12 K and magnetically order at about 0.4 K.

Single crystal alloy samples Lu<sub>1-x</sub>Yb<sub>x</sub>Ni<sub>2</sub>B<sub>2</sub>C have been used to explore the transition from superconductivity through single-impurity Kondo behavior to Kondo lattice heavy-fermion behavior from  $x = 0$  to  $x = 1$  through transport (resistivity and thermopower) [82, 83] and thermodynamic (susceptibility and specific heat) measurements [83, 84]. The suppression of  $T_C$  with Yb substitution does not scale with the de Gennes factor as would be expected from the Abrikosov-Gor'kov theory of magnetic pair breaking [85]. For example, the suppression rate of  $T_C$  at small concentrations  $x$  is 75 times higher for Yb than for Gd [86]. Recent studies [83, 84] indicate that the Kondo temperature varies strongly

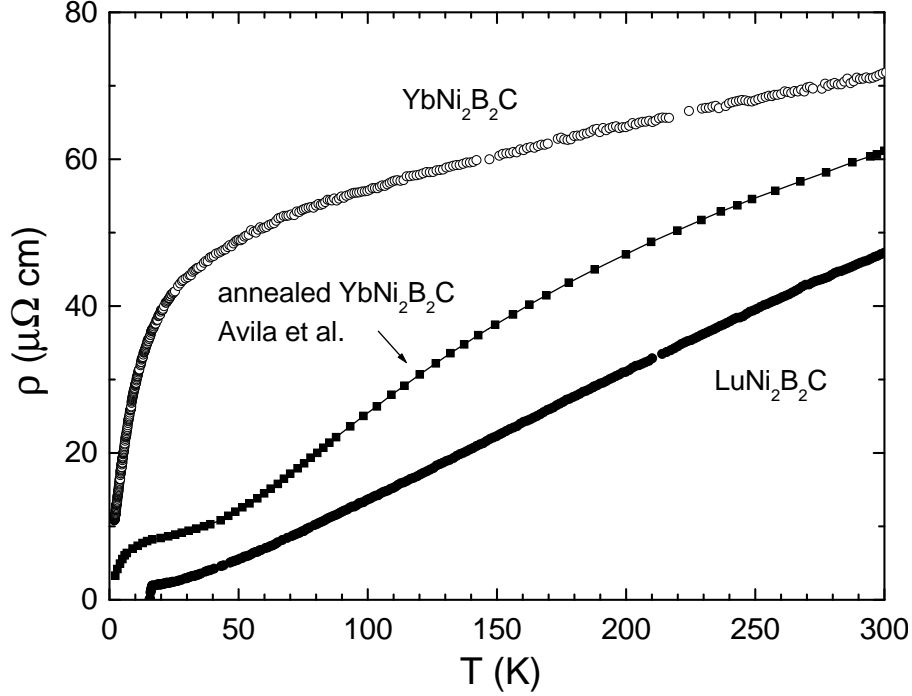


FIG. 17: Temperature dependences of resistivity for  $\text{YbNi}_2\text{B}_2\text{C}$  and  $\text{LuNi}_2\text{B}_2\text{C}$ . The data of Avila *et al.* [88] show  $\rho(T)$  for a single crystal  $\text{YbNi}_2\text{B}_2\text{C}$  annealed for 150 hours at  $950^\circ\text{C}$ .

with Yb concentration  $x$  and that the rapid suppression of  $T_C$  with Yb concentration is consistent with Müller-Hartmann and Zittartz theory [87] for superconducting Kondo systems with spin  $1/2$  and  $T_K/T_C \approx 10^3$ .

Although thermopower and resistivity measurements have been reported for the Lu–Yb borocarbide alloys, the thermal conductivity has only been reported [16] for  $\text{YbNi}_2\text{B}_2\text{C}$ . To illustrate the behavior of this system, the *ab*-plane resistivity, thermopower and thermal conductivity taken from Ref. [16] for an unannealed single crystal sample are shown in Figs. 17, 18, and 19, respectively. The resistivity of a single crystal sample of  $\text{LuNi}_2\text{B}_2\text{C}$  and that of the annealed  $\text{YbNi}_2\text{B}_2\text{C}$  sample [88] are also shown in Fig. 17 for comparison. At high temperature the resistivity varies approximately linearly with temperature and is large in magnitude compared to most metals. The magnitude of the room-temperature resistivity of this sample is about one-fourth of that for the polycrystalline sample in Ref. [80] and one-half of that for the single crystal sample in Ref. [79]. The large variations in the room temperature resistivity suggest unusual disorder effects. The room temperature resistivity for these unannealed Yb-based samples are all much larger than that for  $\text{R} = \text{Lu}$ , or even for the magnetic borocarbides of this family. Recent measurements [88] show that, although the thermodynamic properties are independent of the degree of disorder

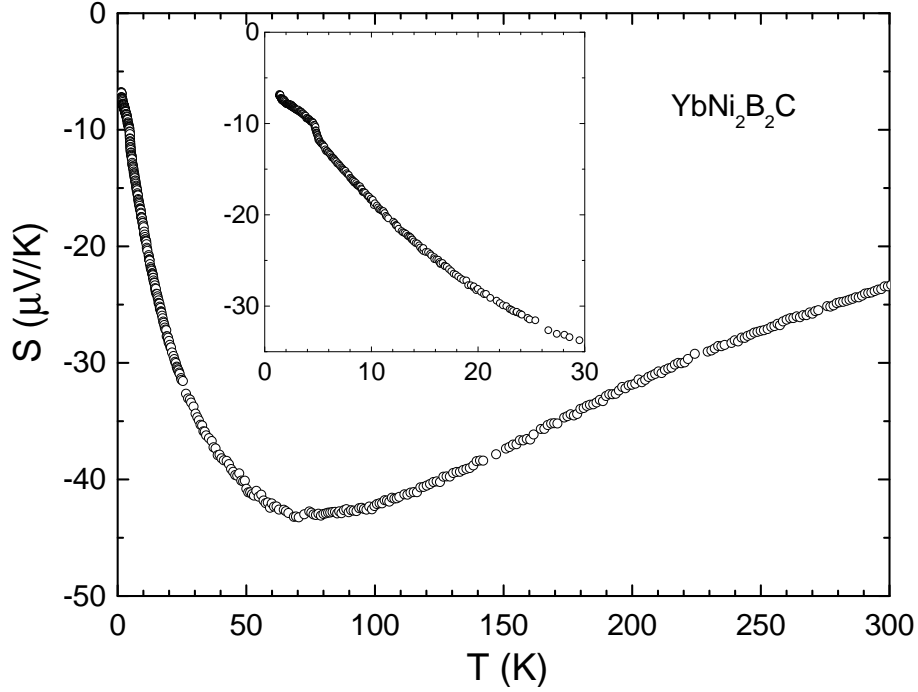


FIG. 18: Temperature dependence of thermo-electric power for  $\text{YbNi}_2\text{B}_2\text{C}$ .

for this heavy fermion compound, the transport properties are very sensitive. Annealing the single crystals for 150 hours at  $950^\circ\text{C}$  reduced the room temperature resistivity for one sample from almost  $100 \mu\Omega \text{ cm}$  to  $60 \mu\Omega \text{ cm}$  and also altered the temperature dependence  $\rho(T)$  appreciably (Fig. 17). The beginning of a Kondo minimum was observed at about 30 K followed by the very sharp decrease in resistance due to coherence around  $T_K$ . Since disorder around the hybridizing Yb site can greatly change the “local” Kondo temperature, these authors interpret the large resistivity and different temperature dependence of  $\rho(T)$  as due to a distribution of local Kondo temperatures [88]. They estimate that only a few percent of sites need to have  $T_K$  much greater than 10 K to explain these differences.

The in-plane thermopower  $S(T)$  in this unannealed single crystal is negative at all temperatures and very large in magnitude compared to the other compounds (see Fig. 18). It decreases linearly with decreasing temperature near room temperature and shows a minimum of about  $-44 \mu\text{V/K}$  near 70 K. At low temperature a distinct shoulder can be seen near 5 K in the insert. This behavior is quite different from that found in the other rare-earth nickel borocarbide family members [49]. These data are in general agreement with other measurements of  $S(T)$  for unannealed single crystals of  $\text{YbNi}_2\text{B}_2\text{C}$  [31, 82, 83]. The magnitude of thermopower, however, is also affected rather strongly by disorder, but the temperature dependence is not much affected. Avila *et al.* [88] report that annealing

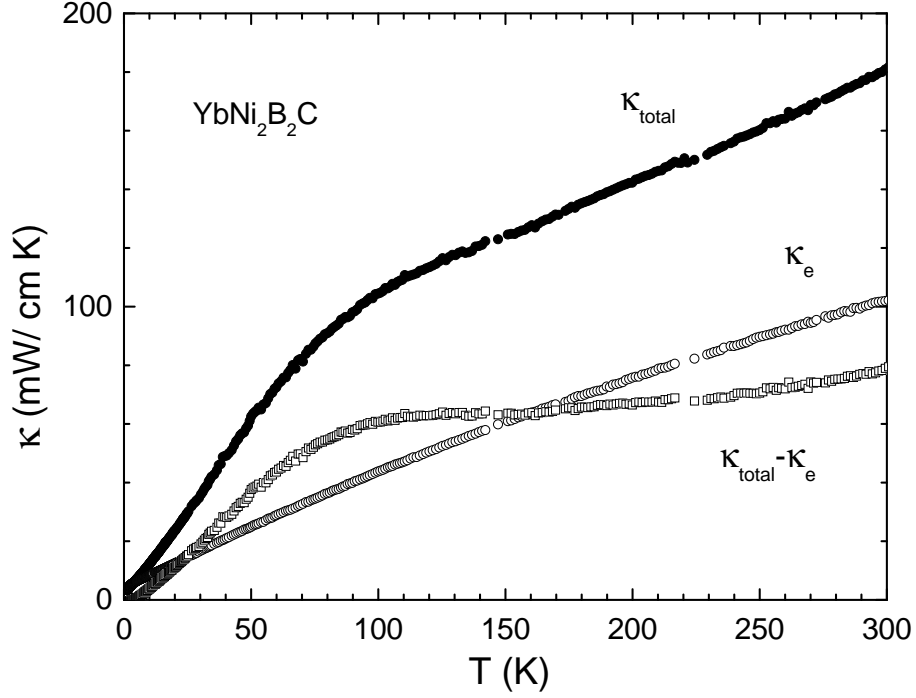


FIG. 19: Temperature dependence of thermal conductivity ( $\kappa_{\text{total}}$ ) for  $\text{YbNi}_2\text{B}_2\text{C}$ . The meaning of  $\kappa_e$  and  $\kappa_{\text{total}} - \kappa_e$  is explained in the main text of the article.

a single crystal for 150 hours at  $950^\circ\text{C}$  reduces the magnitude of  $S(T)$  at the minimum from about  $40\mu\text{V/K}$  to about  $20\mu\text{V/K}$  and moves the minimum to somewhat higher temperature. The influence of disorder at lower temperatures has not been determined since they have measured  $S(T)$  only for  $T \geq 100\text{ K}$ .

The thermal conductivity of this unannealed heavy-fermion sample is shown in Fig. 19. It is rather featureless except for the rapid decrease with decreasing temperature that starts around 100 K. Because of the large resistivity at high temperature the WF law is expected to be valid over much of this temperature range. The phonon contribution inferred from the WF law ( $\kappa_{\text{total}} - \kappa_e$ ) is appreciably smaller at high temperature than that indicated for the other borocarbide samples discussed above, but a similar increase with temperature at high  $T$  is observed for nearly all of the samples. As discussed earlier, this is most likely due to the dominance of PI and/or PE scattering. Although there is no  $\kappa(T)$  data available for well annealed single crystal, one should expect significantly different behavior for the electronic contribution due to the different  $\rho(T)$  dependence reported [88].

## B. Rutheno-Cuprates

Coexistence of superconductivity with ferromagnetism (FM) is one of the fundamental problems in condensed matter physics that has been studied over several decades. Recently, however, coexistence of these two mutually exclusive phenomena have been observed in layered cuprate systems where magnetic order first sets in at temperatures  $T_M$  as high as about 180 K and superconductivity as high as about 50 K. The ratio  $T_M/T_C \approx 4$  is much greater than that described in the intermetallic compounds discussed in sections I or IV A. (See Felner [89] and Lorenz, Xue and Chu [90] for a recent review.) A particularly interesting system where coexistence of weak FM with superconductivity has been reported is  $(R_{1+x}Ce_{1-x})RuSr_2Cu_2O_{10-\delta}$  (Ru-2122 phase), where  $R = Eu$  or  $Gd$ . The compounds, analogous to the Nb-2122 system [91], are related to the  $YBa_2Cu_3O_7$  (123) structure with a fluorite type  $(R_{1+x}Ce_{1-x})O_2$  layer separating the  $CuO_2$  double layers instead of the rare earth Y-layer and with  $RuO_6$  octahedra replacing the  $CuO_4$  squares in the  $CuO$  plane for the 123 high- $T_C$  compound [92]. Because of this fluorite type layer, the successive perovskite blocks are shifted by half a diagonal of the  $ab$ -plane unit cell and the cell is sufficiently long to encompass two formula units per unit cell. The crystal structure is shown in Fig. 1 of the accompanying article by Felner [89] and Fig. 3 in the accompanying article by Lorenz *et al.* [90]. The Ru ion is pentavalent in this compound. Superconductivity is thought to reside primarily in the  $CuO_2$  planes, and the magnetic behavior appears to be associated with the Ru sites. Coexistence of superconductivity and weak FM was first discovered in the Ru-2122 phase for  $R = Eu$  and  $Gd$  [93, 94]. It was also reported for the Ru-1212 phase compound  $GdSr_2RuCu_2O_8$  [95].

The only thermal conductivity measurements reported for this system are for a Ru-2122 sample with  $x = 0.5$  and  $R = Eu$  which has been annealed in pure oxygen at 54 atm. to provide the hole doping in the  $CuO_2$  planes [13]. Consequently, we will focus on coexistence of weak FM and superconductivity in the compound  $(Eu_{1+x}Ce_{1-x})RuSr_2Cu_2O_{10-\delta}$  with  $x = 0.5$  as evidenced by thermopower and thermal conductivity. A detailed review of the other properties of the Ru-2122 phase compounds is given by Felner [89] and by Lorenz *et al.* [90]. They will be only briefly summarized here before discussion of the thermopower and thermal conductivity.

Hole-doping in this system of compounds can be accomplished by either adjusting the  $R^{3+}/Ce^{4+}$  ratio or the oxygen content. The parent insulator compound is assumed to be that for  $\delta = 0$ ,  $x = 0$  [89]. The formal valences then associated with this compound would be  $Eu^{3+}Ce^{4+}Ru^{5+}[Sr^{2+}]_2[Cu^{2+}]_2[O^{2-}]_{10}$ . Superconductivity is observed for  $0.2 \leq x \leq 0.6$  with the optimally doped sample corresponding to  $x = 0.4$ . The

variation of  $T_C$  over this range of  $x$  is only a few Kelvin below that of the optimal value  $T_C = 35$  K (for  $x = 0.4$ ) in the as prepared samples, much less than that expected if all of the carriers were introduced into the  $\text{CuO}_2$  planes. One explanation that has been suggested for this is, that the holes introduced in the  $\text{CuO}_2$  planes by replacing  $\text{Ce}^{4+}$  with  $\text{R}^{3+}$  are partially compensated by a deficiency  $\delta$  in the oxygen content [89]. Neutron diffraction measurements for  $\text{Gd}_{1.3}\text{Ce}_{0.7}\text{RuSr}_2\text{Cu}_2\text{O}_{10-\delta}$  indicate  $\delta = 0.22$  with the deficiency primarily in the fluorite layer and  $\text{RuO}_2$  planes [96]. Recent  $\text{L}_{\text{III}}$ -edge XANES spectra for  $\text{Gd}_{1+x}\text{Ce}_{1-x}\text{RuSr}_2\text{Cu}_2\text{O}_{10}$  with  $x = 0.9$  and  $0.5$ , establish that Ru is pentavalent independent of the Ce concentration [89], i.e. there is no charge transfer to the  $\text{RuO}_2$  layer. In this case the formal valence count would be  $[\text{Gd}_{1+x}\text{Ce}_{1-x}]^{+7-x}\text{Ru}^{+5}[\text{Sr}_2]^{+4}[\text{Cu}_2]^{+4-x+2\delta}[\text{O}_{10-\delta}]^{-20+2\delta}$ . Thus the valence for Cu in this case of  $x = 0.3$  and  $\delta = 0.22$  would be approximately  $+2$  as in the case of  $\text{GdRuSr}_2\text{Cu}_2\text{O}_8$ . Knee *et al.* [96] have suggested that a hole doping mechanism arising from overlap of the  $t_{2g}$  band of Ru and the  $d_{x^2-y^2}$  one of Cu, that is thought to be responsible for superconductivity in  $\text{GdRuSr}_2\text{Cu}_2\text{O}_8$ , may also be responsible for superconductivity in  $\text{Gd}(\text{Eu})_{1+x}\text{Ce}_{1-x}\text{RuSr}_2\text{Cu}_2\text{O}_{10-\delta}$  compounds. Hole doping can also be accomplished by annealing the samples at high temperature and pressure in pure oxygen.  $T_C$  has been raised monotonically from 34 K to as high as 49 K by annealing  $\text{Eu}_{1.5}\text{Ce}_{0.5}\text{RuSr}_2\text{Cu}_2\text{O}_{10-\delta}$  at  $800^\circ\text{C}$  in pure oxygen for 24 hours at pressures up to 150 atm. [97]. Unfortunately, the absolute oxygen content is difficult to determine in this compound. Consequently, neither  $T_C$  as a function of oxygen content nor the location of the excess oxygen in this compound has been systematically determined. Also, the oxygen appears to diffuse back out of these oxygenated samples if held in a vacuum at room temperature.

The magnetic behavior of the  $\text{Eu}_{1+x}\text{Ce}_{1-x}\text{RuSr}_2\text{Cu}_2\text{O}_{10-\delta}$  is also quite unusual [89]. In the high temperature region, Curie-Weiss paramagnetism [ $1/(T - \theta_{\text{CW}})$  law] is observed with an effective moment,  $g\sqrt{S(S+1)}$ , of about  $2.15 \mu_B$  for Ru and a value of  $\theta_{\text{CW}}$  in the interval between 134 K and 146 K, relatively independent of the Ce concentration. This effective moment lies between that of the high spin state for  $\text{Ru}^{5+}$  ( $S = 3/2$ ,  $3.9 \mu_B$ ) and the low-spin state ( $S = 1/2$ ,  $1.7 \mu_B$ ), and the Curie-Weiss temperature  $\theta_{\text{CW}}$  is positive, indicative of a ferromagnetic interaction. The low temperature saturation magnetization ( $gS\mu_B$ ) is only  $0.89 \mu_B/\text{Ru ion}$  compared to the value expected for the high-spin ( $3.0 \mu_B$ ) and low-spin ( $1.0 \mu_B$ ) states for pentavalent Ru. At the temperature  $T_M$  the Ru orders antiferromagnetically as determined by the appearance of non-linearity of in  $M(H)$ . At a lower temperature  $T_{\text{irr}}$ , indicated by the appearance of a remnant magnetization and approximate merging of the field-cooled and zero-field-cooled  $M(T)$  curves, weak FM and irreversibility is produced by canting of the Ru moments as a result of a Dzyaloshinsky-

Moriya type antisymmetric exchange coupling [98] between neighboring Ru moments that is induced by distortion of the  $\text{RuO}_6$  octahedrons. The sharp minimum at 77 K in the temperature derivative of the field-cooled DC susceptibility ( $\chi_{\text{DC}} = M/H$ ) shown in Fig. 20 coincides with this transition for a  $\text{Eu}_{1.5}\text{Ce}_{0.5}\text{RuSr}_2\text{Cu}_2\text{O}_{10-\delta}$  sample that has been annealed at 54 atm. in pure oxygen at 800°C for 12 hours [13]. The sharp rise in the derivative at 45 K coincides with the onset of superconductivity at  $T_{\text{C}}$ . Below this temperature weak FM and superconductivity coexist, presumably on a microscopic scale. No feature indicative of  $T_{\text{M}}$  is observed in  $d\chi_{\text{DC}}/dT$ .<sup>5</sup>

Different possibilities for the structure of coupled inhomogeneous superconducting and magnetic order parameters for weak FM have been previously proposed in the literature: the Fulde-Ferrell-Larkin-Ovchinnikov state [99] where the superconducting order parameter develops a spatial variation with non-zero total momentum, the spiral magnetic (SM) state [100], the spontaneous vortex (SV) state [101], the linearly polarized (LP) state [102], the linearly oscillating vortex (LOV) state [103], and the spiral magnetic vortex (SMV) state [103]. Sonin and Felner [104] have argued that the predicted SV phase [101] is the most likely candidate to describe this state.

The temperatures  $T_{\text{M}}$  and  $T_{\text{irr}}$  depend rather strongly on the doping, and even on the method of doping.  $T_{\text{M}}$  and  $T_{\text{irr}}$  decrease approximately linearly with the reduction  $x$  in Ce content for the as prepared samples [89]. This corresponds to adding holes to the  $\text{CuO}_2$  layer, even though they may be partially compensated by an induced oxygen deficiency. As previously noted, there is an optimal doping for  $x = 0.4$  which gives the maximum in  $T_{\text{C}}$ . If the hole doping via Ce arises from overlap of the Ru and Cu  $d$ -bands, the magnetic behavior of Ru may be band magnetism instead of localized moments [96]. This would be consistent with the differences in the observed saturation moment and effective moment from those expected for  $\text{Ru}^{5+}$ . It is also consistent with the absence of magnetic peaks in the neutron scattering measurements [89, 96]. On the other hand, the effects of doping by annealing in oxygen appear to be quite dependent on the Ce concentration. For the parent composition  $x = 0$ , there appears to be little effect on  $T_{\text{M}}$  and  $T_{\text{irr}}$  [89]. For  $x = 0.5$ , however, both  $T_{\text{M}}$  and  $T_{\text{irr}}$  appear to be enhanced [97]. As

---

<sup>5</sup> Note that a totally different explanation of the magnetic behavior for this type of compound has been suggested by Lorenz *et al.* [90]. They suggest that there is a mesoscopic phase separation between the FM and the AFM species with superconductivity existing only in the AFM grains separated by nanoscale FM domains. Superconductivity would develop in the AFM domains which are Josephson coupled across the FM regions. The onset of the intergrain superconductivity is then expected to be the result of a phase-lock transition of an array of Josephson junctions rather than coexistence of superconductivity with ferromagnetism.

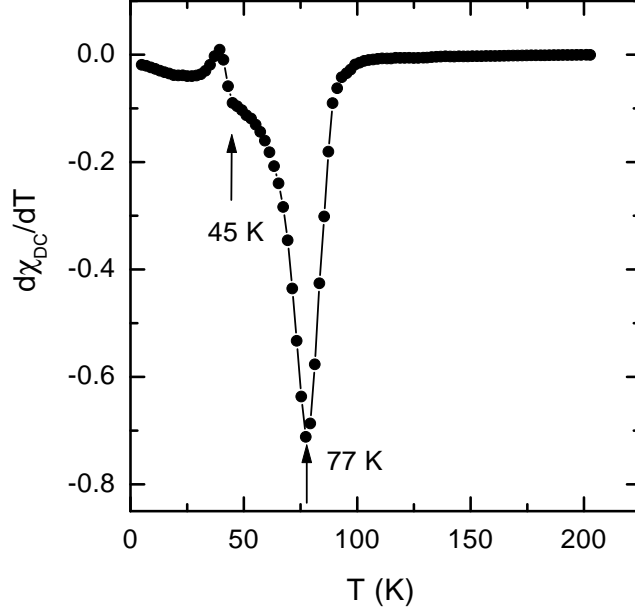


FIG. 20: Derivative of the field-cooled (FC) DC-susceptibility  $d\chi_{\text{DC}}/dT$  [ $\chi_{\text{DC}} = M/H$  was recorded at  $H = 50$  Oe] as a function of temperature  $T$  for an oxygenated  $\text{Eu}_{1.5}\text{Ce}_{0.5}\text{RuSr}_2\text{Cu}_2\text{O}_{10-\delta}$  sample (taken from Ref. [13]). The maximum value in the magnitude at about 77K, very near the point where the zero-field-cooled (ZFC) and FC curves for  $\chi_{\text{DC}}$  approximately appear to merge, is identified as the irreversibility temperature  $T_{\text{irr}}$ . The onset of superconductivity is identified as the sharp break in  $d\chi_{\text{DC}}/dT$  at about 45K. The onset of antiferromagnetic order  $T_{\text{M}}$  determined by the appearance of non-linearity in the  $M(H)$  curves at  $T_{\text{M}} = 180$  K does not produce an observable feature in  $d\chi_{\text{DC}}/dT$ .

previously mentioned,  $T_{\text{C}}$  for this value of  $x$  was significantly enhanced by annealing in oxygen. Thus the effects of doping either by reducing the Ce concentration or changing the oxygen composition by annealing at high pressure are quite different, presumably due to the fact that superconductivity resides in the  $\text{CuO}_2$  planes and the magnetic order resides in the  $\text{RuO}_2$  plane.

The thermopower  $S(T)$  and thermal conductivity  $\kappa(T)$  for the same sample [13] described in Fig. 20 is shown as a function of temperature in Fig. 21. For this sample,  $T_{\text{M}}$  and  $T_{\text{irr}}$  are 180 K and 77 K, respectively. The thermopower is positive over the entire temperature range, consistent with hole charge carriers, and the thermal conductivity is relatively small, characteristic of a pressed powder sample. There is a sharp break in the slope of  $S(T)$  at  $T = 45$  K, precisely the temperature indicated in Fig. 20 for  $T_{\text{C}}$ . The thermopower drops rapidly below this temperature, but it does not go to zero until about 29 K, as might be expected for a granular superconductor. The behavior of the

thermal conductivity near  $T_C$  is quite unusual, in that  $\kappa(T)$  increases by about 30% in an interval of about 1 K at 48 K. Since  $\kappa(T)$  and  $S(T)$  were measured simultaneously, this 3 K difference between their indicated values of  $T_C$  is probably not an experimental artifact. Two additional small reproducible features are seen in both  $S(T)$  and  $\kappa(T)$ , one at  $T_M = 180$  K, which corresponds to other indications of  $T_M$  for the sample [13], and one at  $T^* = 145$  K, which does not coincide with any other reported magnetic or structural anomalies for this compound. An additional feature in  $\kappa(T)$  is seen, a small shoulder with onset at  $T_s = 13$  K. Below about 5 K, the thermal conductivity begins to decrease rapidly.

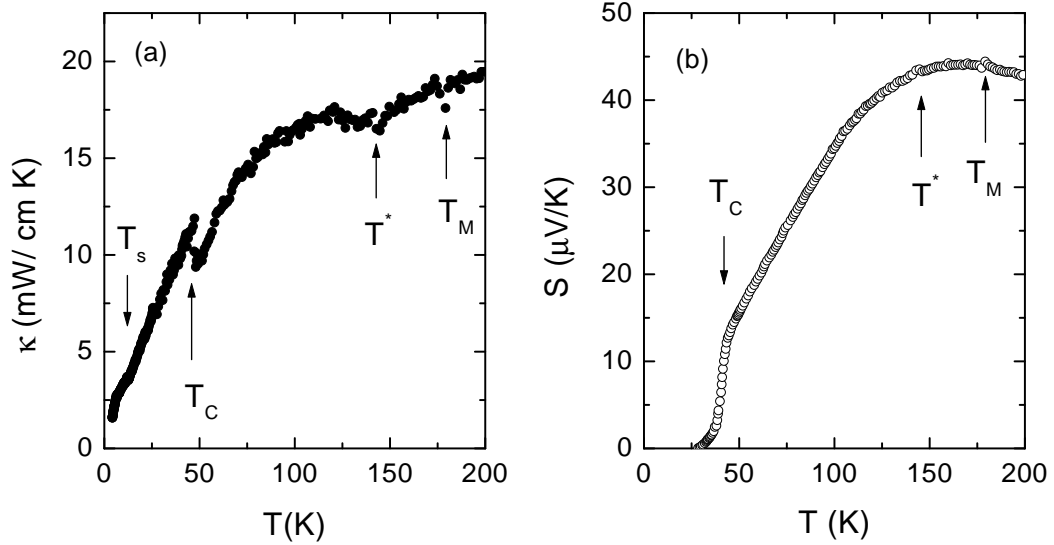


FIG. 21: Thermal conductivity  $\kappa(T)$  (a) and thermopower  $S(T)$  (b) as a function of temperature  $T$  for the same  $\text{Eu}_{1.5}\text{Ce}_{0.5}\text{RuSr}_2\text{Cu}_2\text{O}_{10-\delta}$  sample of Fig. 20 (also taken from Ref. [13]). A small feature in both  $S(T)$  and  $\kappa(T)$  at 180 K matches with the antiferromagnetic ordering temperature  $T_M$ , but no feature corresponding to  $T_{\text{irr}}$  near 77 K is seen in either  $S(T)$  or  $\kappa(T)$ . The superconducting transition temperature  $T_C$  is identified as the sharp change in the slope in  $S(T)$  at 45 K (coincidental with that determined from  $d\chi_{\text{DC}}/dT$  in Fig. 20) and as the abrupt jump in  $\kappa(T)$  at 48 K. The small, reproducible feature in both  $\kappa(T)$  and  $S(T)$  at  $T^* = 145$  K does not match with any yet reported magnetic or structural transitions for this compound.

The most interesting feature is the abrupt 30% increase in  $\kappa(T)$  at 48 K. As discussed in Sec. IIID above, the thermal conductivity for an ordinary superconductor can either increase or decrease at  $T_C$ , dependent on the dominant heat carrier and scattering mechanism. If the dominant carriers are phonons and the scattering mechanism is due primarily to electrons,  $\kappa(T)$  can increase below  $T_C$  as the normal electrons are frozen out. If the

electronic component of  $\kappa$  dominates at  $T_C$ , an increase in  $\kappa$  is not expected at  $T_C$  since the electronic part decreases below  $T_C$ , as illustrated in Fig. 2. The freezing out of the normal electrons is generally very gradual because the conventional superconducting transition in the absence of a magnetic field is second order. Thus, the narrow temperature interval ( $\simeq 1$  K) for the jump is particularly surprising. This behavior is quite distinct from any previously reported for high- $T_C$  superconductors [1], which do, however, exhibit a much broader rise in  $\kappa(T)$  below  $T_C$ .

Onset of magnetic order generally leads to a significant increase in  $\kappa(T)$  due to loss of scattering of the electrons by spin disorder. This is particularly pronounced in the data for  $\text{HoNi}_2\text{B}_2\text{C}$ ,  $\text{DyNi}_2\text{B}_2\text{C}$  and  $\text{TmNi}_2\text{B}_2\text{C}$  (though it is probably due to a new heat carrier, spin waves, for the latter compound) as discussed in Sec. IV A above (see Figs. 4, 6, and 10). In contrast, there is no strong signature of magnetic order in  $\kappa(T)$  near the AFM ordering temperature  $T_N$  or the onset of weak FM at  $T_{\text{WF}}$  for  $\text{ErNi}_2\text{B}_2\text{C}$  (see Fig. 8) which are both well below  $T_C$ . For this rutheno-cuprate sample, however, AFM order has already set in at  $T_M = 180$  K and weak FM at  $T_{\text{irr}} = 77$  K. Based on the results described earlier for  $\text{DyNi}_2\text{B}_2\text{C}$  and  $\text{TbNi}_2\text{B}_2\text{C}$  (see Figs. 4 and 14), the magnetic ordering is expected to affect the scattering of the electrons primarily, with little effect on the phonon scattering. Unfortunately, resistivity was not measured for this rutheno-cuprate sample to provide an estimate of the electronic contribution to  $\kappa(T)$  through the WF law. Such an estimate probably would have been very inaccurate in any case, however, since it is less likely that this law would be valid at the higher  $T_C$  values.

The shoulder between 5 K and 13 K in  $\kappa(T)$  is perhaps related to the similar "phonon" peak seen in  $\kappa(T)$  for the  $\text{Lu(Y)Ni}_2\text{B}_2\text{C}$  samples discussed in Sec. IV A above (see Fig. 12). It is quite probable that this peak for these borocarbides arises from the phonon channel as the normal electrons become less effective phonon scatterers at temperatures well below  $T_C$ . A similar interpretation would imply a strong electron-phonon interaction in the rutheno-cuprate. It would also imply a very reduced density of normal electrons in the regions where the magnetic order parameter was strong since the shoulder was washed out by the introduction of vortices with their normal cores in  $\text{YNi}_2\text{B}_2\text{C}$  through application of a magnetic field [56]. The breadth of the drop to zero of  $S(T)$  at 29 K, well below the onset of superconductivity at 45 K, may be the result of inhomogeneity of the doping of the sample leading to a percolation transition or to the Josephson junction array model suggested by Lorenz *et al.* [90]. The abrupt jump in  $\kappa(T)$  at 48 K would appear to be inconsistent either with a percolation transition or the Josephson junction array model, however. Alternatively, it may result from vortices in the superconducting state or another, more complicated state of the coupled superconducting and magnetic

order parameters.

The thermal conductivity measurements cannot determine the detailed nature of the phase that leads to this abrupt jump in  $\kappa$  near  $T_C$ . The jump does strongly suggest that the transition is first order. This may be due to the influence of the internal field on the superconducting state, a significant change in the magnetic order to accomodate coexistence of both types of order, or the appearance of vortices in the superconducting state to accommodate weak FM. These rutheno-cuprates do appear to be quite unique in their behavior, however. The fact that magnetic order first sets in at a temperature almost four times that of  $T_C$  is fascinating. A magnetic transition at 48 K to a new magnetic state that would permit the superconducting phase transition at 45 K would appear to be consistent with the abrupt jump in  $\kappa$  and the 3 K difference in the sharp features near  $T_C$  seen in the simultaneous  $S(T)$  and  $\kappa(T)$  measurements. Major efforts are needed to grow better quality and better characterized materials so that techniques that probe this new state on a microscopic scale can be more readily employed.

## V. CONCLUSION

In conclusion, we have presented here an overview of the thermal conductivity behavior in magnetic superconductors with particular emphasis on the rare earth nickel borocarbide intermetallic compounds and the 2122 rare earth rutheno-cuprates. The borocarbide family of intermetallics is of importance because of the availability of high quality single crystal samples and the large variety of phenomena - only superconductivity, coexistence of superconductivity and magnetic order, only magnetic order, and heavy fermion behavior - within the same family of compounds with identical crystal structure and similar electronic structure. To complete the picture of thermal conductivity in this family, a description of the measurements of  $\kappa(T)$  was given for all members for which single crystal samples were available, not just the four magnetic superconductors. Although only limited thermal conductivity data is available, the oxygen rich  $\text{Eu}_{1.5}\text{Ce}_{0.5}\text{RuSr}_2\text{Cu}_2\text{O}_{10+\delta}$  compound may be unique as a compound that exhibits a coupled transition to weak ferromagnetism and superconductivity at a surprisingly high temperature ( $\approx 45$  K) and onset of AFM near 200 K.

It follows from the results presented that thermal conductivity study is a rather powerful technique for revealing the fundamental properties of these complex compounds. The technique is especially useful for study of phase transitions. It is clear, however, that any single method of investigation alone cannot give a complete picture of the physical properties and phenomena, which are inherent in some complex compound. The ther-

mal conductivity studies can, however, amplify the data, obtained by other experimental methods (such as neutron diffraction, resistivity, specific heat, thermopower and other techniques) and give food for thoughts on important questions for theoretical investigations.

### Acknowledgments

Much of the work reported here was supported in part by the Robert A. Welch Foundation (Grant A-0514), the Telecommunications and Informatics Task Force at Texas A&M University, the Texas Center for Superconductivity and Advanced Materials at the University of Houston (TCSAM) and the National Science Foundation (Grants DMR-0103455 and DMR-0111682).

- 
- [1] C. Uher in *Physical Properties of High Temperature Superconductors III*, edited by D. M. Ginsberg (World Scientific, Singapore, 1992) pp. 159-283.
  - [2] C. Proust, E. Boaknin, R. W. Hill, L. Taillefer, and A. P. Mackenzie, *Phys. Rev. Lett.* **89**, 147003 (2002).
  - [3] R. W. Hill, C. Proust, L. Taillefer, P. Fournier, and R. L. Greene, *Nature (London)* **414**, 711 (2002).
  - [4] Q. Si, *Physica C* **364-365**, 9 (2001).
  - [5] M. B. Maple in *Advances in Superconductivity*, edited by B. Deaver and J. Ruvalds (Plenum, NY, 1982) pp. 279-346.
  - [6] L. N. Bulaevskii, A. I. Buzdin, M. Kulić, and S. V. Panjukov, *Adv. Phys.* **34**, 175 (1985).
  - [7] Ø. Fischer in *Ferromagnetic Materials*, Vol. 5, edited by K. H. J. Buschow and E. P. Wohlfarth (North-Holland, Amsterdam, 1990) pp. 465-550.
  - [8] C. Mazumdar, R. Nagarajan, C. Godart, L.C. Gupta, M. Latroche, S. K. Dhar, C. L. Clement, B. D. Padalia, and R. Vijayaraghavan, *Solid State Commun.* **87**, 413 (1993).
  - [9] R. Nagarajan, C. Mazumdar, Z. Hossain, S. K. Dhar, K. V. Gopalakrishnan, L. C. Gupta, C. Godart, B. D. Padalia, and R. Vijayaraghavan, *Phys. Rev. Lett.* **72**, 274 (1994).
  - [10] R. J. Cava, H. Takagi, B. Batlogg, H. W. Zandbergen, J. J. Krajewski, W. F. Peck, Jr., R. B. van Dover, R. J. Felder, T. Siegrist, K. Mizahashi, J. O. Lee, H. Eisaki, S. A. Carter, and S. Uchida, *Nature (London)* **367**, 146 (1994).
  - [11] R. J. Cava, H. Takagi, H. W. Zandbergen, J. J. Krajewski, W. F. Peck Jr., T. Siegrist, B. Batlogg, R. B. van Dover, R. J. Felder, K. Mizuhashi, J. O. Lee, H. Eisaki, and S. Uchida,

- Nature (London) **367**, 252 (1994).
- [12] M. Xu, P. C. Canfield, J. E. Ostenson, D. K. Finnemore, B. K. Cho, Z. R. Wang, and D. C. Johnston, *Physica C* **227**, 321 (1994).
  - [13] B. D. Hennings, K. D. D. Rathnayaka, D. G. Naugle, and I. Felner, *Physica C* **370**, 253 (2002).
  - [14] J. E. Parrot and A. D. Stuckes, *Thermal conductivity of Solids* (Pion, London, 1975).
  - [15] G. E. Childs, L. J. Ericks, and R. L. Powell, *Thermal conductivity of Solids at Room Temperature and Below: A Review and Compilation of the Literature*, NBS Monograph 131 (Nat. Bur. Stand., Washington, D. C., 1973).
  - [16] B. D. Hennings in *Thermal Transport in Single-Crystal Rare Earth Nickel Borocarbides*, Ph. D. Dissertation, Texas A&M University (2002), unpublished.
  - [17] J. M. Ziman, *Electrons and Phonons* (Oxford University Press, London, 1960).
  - [18] F. J. Blatt, *Physics of Electronic Conduction in Solids* (McGraw-Hill, 1968).
  - [19] N. W. Ashcroft and N. D. Mermin, *Solid State Physics* (Holt, Rinehart and Winston, New York, 1976)
  - [20] R. Berman, *Thermal Conduction in Solids* (Oxford University Press, London, 1979).
  - [21] B. T. Geilikman, *Sov. Phys. JETP* **7**, 721 (1958).
  - [22] J. Bardeen, G. Rickayzen, and L. Tewordt, *Phys. Rev.* **113**, 982 (1959).
  - [23] B. T. Gelikman and V. Z. Kresin, *Sov. Phys. JETP* **9**, 677 (1959).
  - [24] L. Tewordt, *Phys. Rev.* **129**, 657 (1963).
  - [25] B. T. Geilikman and V. Z. Kresin, *Kinetic and Nonsteady-Effects in Superconductors* (Wiley, New York, 1974).
  - [26] G. Rickayzen, in *Superconductivity*, edited by R. Parks (Marcell Dekker, New York, 1969), Vol. 1, Chapt. 2.
  - [27] D. M. Ginsberg and L. C. Hebel, *ibid.*, Vol. 1, Chapt. 4.
  - [28] G. K. White, *Experimental Techniques in Low-Temperature Physics* (Oxford University Press, London, 1959).
  - [29] K. Mendelssohn and J. Olsen, *Proc. Phys. Soc.* **63A**, 2 (1950).
  - [30] G. Hilscher and H. Michor, in *Studies of High Temperature Superconductors*, edited by A. Narlikar (Nova Science Publishers, Commack, NY, 1999), Vol. 28, pp 241-286.
  - [31] D. G. Naugle, K. D. D. Rathnayaka and A. K. Bhatnagar, *ibid.*, Vol. 28, pp 189-239.
  - [32] S.-L. Drechsler, S. V. Shulga, K.-H. Müller, G. Fuchs, J. Freudenberger, G. Behr, H. Eschrig, L. Schultz, M. S. Golden, H. von Lips, J. Fink, V. N. Narozhnyi, H. Rosner, P. Zahn, A. Gladun, D. Lipp, A. Kreyssig, M. Loewenhaupt, K. Koepernik, K. Winzer, and K. Krug, *Physica C* **317-318**, 117 (1999).

- [33] K.-H. Müller and V. N. Narozhnyi, Rep. Progr. Phys., **64**, 943 (2001).
- [34] T. Siegrist, H. W. Zandbergen, R. J. Cava, J. J. Krajewski, and W. F. Peck, Jr., Nature (London) **367**, 254 (1994).
- [35] L. F. Mattheiss, Phys. Rev. B **49**, 13279 (1994); W. E. Pickett and D. J. Singh, Phys. Rev. Lett. **72**, 3702 (1994); H. Kim, C.-D. Hwang, and J. Ihm, Phys. Rev. B **52**, 4592 (1994); M. Diviš, K. Schwarz, P. Blaha, G. Hilscher, H. Michor, and S. Khmelevskyi, Phys. Rev. B **62**, 6774 (2000).
- [36] E. Pellegrin, C. T. Chen, G. Meigs, R. J. Cava, J. J. Krajewski, and W. F. Peck, Jr., Phys. Rev. B **51**, 16159 (1995); T. Böske, M. Kielwein, M. Knupfer, S. R. Barman, G. Behr, M. Buchgeister, M. S. Golden, and J. Fink, Solid State Commun. **99**, 23 (1996).
- [37] I. R. Fisher, J. R. Cooper, and P. C. Canfield, Phys. Rev. B **56**, 10820 (1997).
- [38] J. W. Lynn, S. Skanthakumar, Q. Huang, S. K. Sinha, Z. Hossain, L. C. Gupta, R. Nagarajan, C. Godart, Phys. Rev. B **55**, 6584 (1997).
- [39] P. Bonville, J. A. Hodges, Z. Hossain, R. Nagarajan, S. K. Dhar, L. C. Gupta, E. Alleno, and C. Godart, Eur. Phys. J. B **11**, 377 (1999).
- [40] P. C. Canfield, S. L. Bud'ko, and B. K. Cho, Physica C **262**, 249 (1996).
- [41] B. K. Cho, P. C. Canfield, and D. C. Johnston, Phys. Rev. B **53**, 8499 (1996); P. Dervnagas, J. Zarestky, C. Stassis, A. I. Goldman, P. C. Canfield, and B. K. Cho, Phys. Rev. B **53**, 8506 (1996).
- [42] P. G. de Gennes, *Superconductivity in metals and alloys* (W. A. Benjamin, New York, 1966).
- [43] W. Baltensperger and S. Strässler, Phys. kondens. Materie **1**, 20 (1963).
- [44] B. Brandow, Phys. Rep. **296**, 1 (1998).
- [45] J. F. Annett, Physica C **317-318**, 1 (1999).
- [46] K. Maki, P. Thalmeier, and H. Won, Phys. Rev. B **65**, 140502(R) (2002).
- [47] P. Mandal and K. Winzer, Solid State Commun. **103**, 679 (1997).
- [48] K. Winzer and K. Krug, in *Rare Earth Transition Metal Borocarbides (Nitrides): Superconducting, Magnetic and Normal State Properties*, edited by K.-H. Müller and V. Narozhnyi (Kluwer, Dordrecht, 2001) pp 63–69.
- [49] K. D. D. Rathnayaka, A. K. Bhatnagar, A. Parasiris, D. G. Naugle, P. C. Canfield, and B. K. Cho, Phys. Rev. B **55**, 8506 (1997); A. K. Bhatnagar, K. D. D. Rathnayaka, D. G. Naugle, and P. C. Canfield, Phys. Rev. B **56**, 437 (1997).
- [50] G. T. Meaden, *Electrical resistance of metals* (Heywood Books, London, 1966).
- [51] R. Nagarajan, in *Rare Earth Transition Metal Borocarbides (Nitrides): Superconducting, Magnetic and Normal State Properties*, edited by K.-H. Müller and V. Narozhnyi (Kluwer,

- Dordrecht, 2001) pp 1–20.
- [52] J. S. Kim, W. W. Kim, and G. R. Stewart, Phys. Rev. B **50**, 3485 (1994); S. A. Carter, B. Batlogg, R. J. Cava, J. J. Krajewskii, W. F. Peck, Jr., and H. Takagi, Phys. Rev. B **50**, 4216 (1994).
  - [53] N. M. Hong, H. Michor, M. Vybornov, T. Holubar, P. Hundegger, W. Perthold, G. Hilscher, and P. Rogl, Physica C **227**, 85 (1994).
  - [54] R. Movshovich, M. F. Hundley, J. D. Thompson, P. C. Canfield, B. K. Cho, and A. V. Chubukov, Physica C **227**, 381 (1994).
  - [55] H. Michor, T. Holubar, C. Dusek, and G. Hilscher, Phys. Rev. B **52**, 16165 (1995).
  - [56] M. Sera, S. Kobayash, M. Hiroi, N. Kobayashi, H. Takeya, and K. Kadowaki, Phys. Rev. B **54**, 3062 (1996).
  - [57] S. Cao, S. Sakai, K. Nishimura, and K. Mori, Physica C **341-348**, 751 (2000).
  - [58] E. Boaknin, R. W. Hill, C. Lupien, L. Taillefer, and P. C. Canfield, Physica C **341-348**, 1845 (2000).
  - [59] B. D. Hennings, K. D. D. Rathnayaka, D. G. Naugle, and P. C. Canfield, Physica C **341-348**, 753 (2000); Physica C **364-365**, 257 (2001).
  - [60] E. Boaknin, R. W. Hill, C. Proust, C. Lupien, L. Taillefer, and P. C. Canfield, Phys. Rev. Lett. **87**, 237001 (2001).
  - [61] B. D. Hennings, D. G. Naugle, and P. C. Canfield, Phys. Rev. B **66**, 214512 (2002).
  - [62] K. Izawa, K. Kamata, Y. Nakajima, Y. Matsuda, T. Watanabe, M. Nohara, H. Takagi, P. Thalmeier, and K. Maki, Phys. Rev. Lett. **89**, 137006 (2002).
  - [63] P. Dervénagas, J. Zarestky, C. Stassis, A. I. Goldman, P. C. Canfield, B. K. Cho, Physica B **212**, 1 (1995); J. P. Sanchez, P. Vulliet, C. Godart, L. C. Gupta, Z. Hossain, and R. Nagarajan, Phys. Rev. B **54**, 9421 (1996); M. S. Lin, J. H. Shieh, Y. B. You, Y. Y. Hsu, J. W. Chen, S. H. Lin, Y. D. Yao, Y. Y. Chen, J. C. Ho, and H. C. Ku, Physica C **249**, 403 (1995).
  - [64] E. Gratz and M. J. Zuckermann, in *Handbook of the Physics and Chemistry of Rare Earth*, edited by K. A. Geschneider, Jr. and L. Eyring (North-Holland, Amsterdam, 1982) pp 117–216.
  - [65] P. C. Canfield, B. K. Cho, D. C. Johnston, D. K. Finnemore, and M. F. Hundley, Physica C **230**, 397 (1994).
  - [66] S. A. Carter, B. Batlogg, R. J. Cava, J. J. Krajewski, and W. F. Peck, Jr., Phys. Rev. B **51**, 12644 (1995).
  - [67] L. F. Ribaltchenko, I. K. Yanson, A. G. M. Jansen, P. Mandal, P. Wyder, C. V. Tomy, and D. McK. Paul, Physica B **218**, 189 (1996).

- [68] S.-M. Choi, J. W. Lynn, D. Lopez, P.L. Gammel, P. C. Canfield, and S. L. Bud'ko, Phys. Rev. Lett. **87**, 107001 (2001).
- [69] L. J. Chang, C. V. Tomy, D. McK. Paul, and C. Ritter, Phys. Rev. B **54**, 9031 (1996).
- [70] D. G. Naugle, K. D. D. Rathnayaka, K. Clark, and P. C. Canfield, Int. J. Mod. Phys. B **13**, 3715 (1999).
- [71] J. H. Kim and D. H. Wu, Physica C **364-365**, 24 (2001).
- [72] G. J. Suh, F. Borsa, D. R. Torgesson, B. K. Cho, P. C. Canfield, D. C. Johnson, J. Y. Rhee, and B. N. Harmon, Phys. Rev. B **53**, R6022 (1996); I. Felner, J. Magn. Magn. Mater. **157/158**, 622 (1996).
- [73] H. Kawano, H. Yoshizawa, H. Takeya, and K. Kadowaki, Phys. Rev. Lett. **77**, 4628 (1996).
- [74] P. Dervénagas, M. Bullock, J. Zarestky, P. Canfield, B. K. Cho, B. Harmon, A. I. Goldman, and C. Stassis, Phys. Rev. B **52**, R9839 (1995); C. Stassis, M. Bullock, J. Zarestky, P. Canfield, A. I. Goldman, G. Shirane, and S. M. Shapiro, Phys. Rev. B **55**, R8678 (1997).
- [75] C. V. Tomy, L. A. Afalfiz, M. R. Lees, J. M. Martin, D. McK. Paul, and D. T. Adroja, Phys. Rev. B **53**, 307 (1996); C. V. Tomy, L. J. Chang, D. McK. Paul, and C. Ritter, Physica B **230-232**, 872 (1997).
- [76] C. Detlefs, A. I. Goldman, C. Stassis, P. C. Canfield, B. K. Cho, J. P. Hill, and D. Gibbs, Phys. Rev. B **53**, 6355 (1996).
- [77] K. Tomala, J. P. Sanchez, P. Vulliet, P. C. Canfield, Z. Drzazga, and A. Winiarska, Phys. Rev. B **58**, 8534 (1998).
- [78] A. Lacerda, A. Yatskar, G. M. Schmiedeshoff, W. P. Beyermann, and P. C. Canfield, Phil. Mag. B **74**, 641 (1996).
- [79] A. Yatskar, N. K. Budraa, W. P. Beyermann, C. P. Canfield, and S. L. Bud'ko, Phys. Rev. B **54**, 3772 (1996).
- [80] S. K. Dhar, R. Nagarajan, Z. Hossain, E. Tominez, C. Godart, L. C. Gupta, and R. Vijayaraghavan, Solid State Commun. **98**, 985 (1996).
- [81] A. T. Boothroyd, J. P. Barrat, P. Bonville, P. C. Canfield, A. Murani, A. R. Wildes, and R. I. Bewley, preprint, cond-mat/0211277.
- [82] K. D. D. Rathnayaka, D. G. Naugle, Shi Li, M. C. de Andrade, R. P. Dickey, A. Amann, M. B. Maple, S. L. Bud'ko, P. C. Canfield, and W. P. Beyermann, Int. J. Mod. Phys. B **13**, 3725 (1999).
- [83] Preprint, Shi Li, M. C. de Andrade, R. P. Dickey, A. Amann, M. B. Maple, K. D. D. Rathnayaka, D. G. Naugle, S. L. Bud'ko, P. C. Canfield, and W. P. Beyermann.
- [84] Preprint, E. J. Freeman, C. Sirvent, Shi Li, R. P. Dickey, A. Amann, N. A. Frederick, M. B. Maple, K. D. D. Rathnayaka, D. G. Naugle, S. L. Bud'ko, P. C. Canfield, and W. P.

Beyermann.

- [85] S. L. Bud'ko, P. C. Canfield, A. Yatskar, and W. P. Beyermann, *Physica B* **230-232**, 859 (1997).
- [86] B. K. Cho, P. C. Canfield, and D. C. Johnston, *Phys. Rev. Lett.* **77**, 163 (1996).
- [87] E. Müller-Hartmann and J. Zittartz, *Z. Phys.* **234**, 58 (1970); *Solid State Commun.* **11**, 401 (1972).
- [88] M. A. Avila, S. L. Bud'ko, and P. C. Canfield, *Phys. Rev. B* **66**, 132504 (2002).
- [89] I. Felner, in this volume of *Studies of High Temperature Superconductors*, V. A. Narlikar, ed. (Nova Science Publ., N.Y.); preprint cond-mat/0211533.
- [90] B. Lorenz, Y. Y. Xue, and C. W. Chu, in this volume of *Studies of High Temperature Superconductors*, V. A. Narlikar, ed. (Nova Science Publ., N.Y.); preprint cond-mat/0211492.
- [91] R. J. Cava, J. J. Krajewski, H. Takagi, H. W. Zandbergen, R. B. van Dover, W. F. Peck Jr. and B. Hessen, *Physica C* **191**, 237 (1992).
- [92] L. Bauernfeind, W. Widder and H. F. Braun, *Physica C* **254**, 151 (1995).
- [93] I. Felner, U. Asaf, Y. Levi and O. Millo, *Phys. Rev. B* **55**, R3374 (1997); I. Felner, U. Asaf, Y. Levi and O. Millo, *Physica C* **334**, 141 (2000).
- [94] Y. Y. Xue, B. Lorenz, A. Baikalov, D. H. Cao, Z. G. Li and C. W. Chu, *Phys. Rev. B* **66**, 014503 (2002).
- [95] C. Bernhard, J. L. Tallon, Ch. Niedermayer, Th. Blasius, A. Golnick, B. Brücher, R. K. Kremer, D. R. Noakes, C. E. Stronach and E. J. Ansaldo, *Phys. Rev. B* **59**, 14099 (1999); J. L. Tallon, J. W. Loram, G. V. M. Williams and C. Bernhard, *Phys. Rev. B* **61**, R6471 (2000); C. Bernhard, J. L. Tallon, E. Brücher and R. K. Kremer, *Phys. Rev. B* **61**, R14960 (2000).
- [96] C. S. Knee, B. D. Rainford and M. T. Weller, *J. Mater. Chem.* **10**, 2445 (2000).
- [97] I. Felner, U. Asaf, Y. Levi and O. Millo, *Int. J. Mod. Phys. B* **13**, 3650 (1999).
- [98] J. Dzyaloshinski, *J. Phys. Chem. Solids* **4**, 241 (1958).
- [99] P. Fulde and R. A. Ferrell, *Phys. Rev.* **135**, A550 (1964); A. I. Larkin and Yu. N. Ovchinnikov, *Sov. Phys. JETP* **20**, 762 (1965).
- [100] E. I. Blount and C. M. Varma, *Phys. Rev. Lett.* **42**, 1079 (1979).
- [101] C. G. Kuper, M. Revzen, and A. Ron, *Phys. Rev. Lett.* **44**, 1545 (1980).
- [102] H. S. Greenside, E. I. Blount and C. M. Varma, *Phys. Rev. Lett.* **46**, 49 (1981).
- [103] C. R. Hu and T. E. Ham, *Physica B&C* **108**, 1041 (1981).
- [104] E. B. Sonin and I. Felner, *Phys. Rev. B* **57**, R14000 (1998).